CHALMERS
UNIVERSITY OF TECHNOLOGY

Modeling and Control of Aeration in a Wastewater Treatment Plant

Master's thesis in Systems control and mechatronics and Sustainable energy systems

NILS LARSSON
DANIEL SVENSSON

DEPARTMENT OF ELECTRICAL ENGINEERING

CHALMERS UNIVERSITY OF TECHNOLOGY
Gothenburg, Sweden 2025
www.chalmers.se

Master's thesis 2025

Modeling and Control of Aeration in a Wastewater Treatment Plant

Nils Larsson
Daniel Svensson

CHALMERS
UNIVERSITY OF TECHNOLOGY

Department of Electrical engineering
Division of Systems and control
Chalmers University of Technology
Gothenburg, Sweden 2025

Modeling and Control of Aeration in a Wastewater Treatment Plant
NILS LARSSON
DANIEL SVENSSON

Supervisor: Carl Ressel, Solvina AB
Examiner: Veronica Olesen, Systems and Control, Electrical engineering

Master's Thesis 2025
Department of Electrical engineering
Division of Systems and control
Chalmers University of Technology
SE-412 96 Gothenburg
Telephone +46 31 772 1000

Cover: Biological treatment basins at Käppala WWTP. Provided by Käppalaförbundet, used with permission.

Typeset in LaTeX
Gothenburg, Sweden 2025

Modeling and Control of Aeration in a Wastewater Treatment Plant
NILS LARSSON
DANIEL SVENSSON
Department of Electrical Engineering
Chalmers University of Technology

Abstract

In this thesis, several modified control strategies for aeration control in a wastewater treatment plant are implemented. Their performance with focus on energy consumption and airflow pattern is evaluated and compared to the existing control system. In the wastewater treatment process (WWTP), the biological step is where oxygen is needed to regulate the ammonium levels in the effluent water, which can therefore be controlled with the airflow. A model of a wastewater treatment plant (WWTP) was built in Simulink to simulate the plant and evaluate the different control strategies. Time periods for real-world data were selected and used, both for evaluation of the model accuracy and the control system performance. The final conclusions made are that there is room for improvement of the control system with for example feedforward of the inflow rate. However, improvements are limited to the daily variations and cannot help suppress the very high spikes in ammonia concentration seen a few times a year. The likely cause being that these are present due to capacity constraints being reached in the system. Energy consumption was also not substantially lowered by the modified control strategies and therefore, they are not recommended in their current form. Attempts were also made to implement an LQG controller. However, an LQG controller is based on a linear model of the system, and the WWTP is highly nonlinear with global stability concerns. Thus, an LQG controller was not feasible for this system.

Keywords: WWTP, modeling, control theory, ASM1, gain scheduling, LQG, feedforward, feedback

Acknowledgements

We would like to thank our supervisor Carl Ressel, Solvina AB. For his advise, support and consultation which has been invaluable throughout the process. We would also like to thank Veronica Olesen for her continued support and advise, helping us stay on track. Thanks to all the colleges at Solvina for the inclusive and supportive environment.

Nils Larsson & Daniel Svensson, Gothenburg, May 2025

List of Acronyms

Below is the list of acronyms that have been used throughout this thesis listed in alphabetical order:

BOD	Biological Oxygen Demand
COD	Chemical Oxygen Demand
DO	Dissolved Oxygen
FB	Feedback
FF	Feedforward
GS	Gain Scheduling
LQE	Linear Quadratic Estimator
LQG	Linear Quadratic Gaussian
LQR	Linear Quadratic Regulator
ODE	Ordinary Differential Equation
WWTP	Waste Water Treatment Plant

Nomenclature

Below is the nomenclature of indices and variables that have been used throughout this thesis.

Indices

s	Index for step in Laplace domain
t	Index for time step

Variables

Q	volumetric flow rate
V	volume
J	material flux
DO_{sat}	saturated oxygen concentration
T	temperature
S	soluble concentration
X	particulate concentration
DO	dissolved oxygen
NH	ammonia concentration
T	temperature
Q_L	inlet airflow from blowers
K_La	oxygen transfer rate
rpm	rotations per minute

Contents

1

Introduction

The focus of this thesis is to explore new control strategies for aeration control in a wastewater treatment plant with the goal of reducing energy consumption. Together with Solvina AB, options for improving the control strategy have been explored.

1.1 Background

Waste water treatment plants (WWTP) play a pivotal role in modern society by circulating and cleaning resources, as they are relied upon to clean wastewater from cities and towns to keep the water environment free from pollution. This leads to them having to process large volumes of water, around 4 000 000 m^3 per day. The energy consumption of Swedish water treatment plants was estimated to be on average around 630 GWh/year, where 24% is used in aeration [1]. Hence, making the aerators more efficient is one important way to save energy and reduce energy costs.

Aeration is part of the treatment process, where microorganisms are used to lower the levels of ammonia in the effluent wastewater [2]. These microorganisms need oxygen and therefore air is supplied to the basins containing them. The air is supplied by compressors, usually several in parallel to keep them operating close to design point even with changing loads, in order to keep the efficiency high. An unstable and poorly performing control system (controlling the aeration) tends to lead to the compressors getting damaged, needing maintenance and/or needing to be replaced prematurely.

A wastewater treatment plant is a system with large time constants, which means that it takes a long time for a volume in the inlet to reach the outlet. This leads to long response times, which tends to make the system more difficult to control. One of the main problems in designing controllers for the aeration of WWTPs is that the systems are big and difficult to model with many unpredictable disturbances, such as weather and seasons which impact the flow and temperature of the water. Due to these complex and sometimes nonintuitive interactions, having a model remains essential to conduct tests and evaluations on, as suitable control design plays a central role in increasing the energy efficiency of the WWTPs [2]. Given that modeling is one of the many challenges that will need to be tackled in order to find a control strategy that is able to improve system stability and consequently lower energy costs for the plant, while still meeting environmental regulations.

1.2 Aim

The aim of this thesis is to develop and investigate a control strategy for the aeration system of a wastewater treatment plant. The control strategy will be analyzed to determine how it affects the operation and energy consumption of the compressors. This should be done by answering the questions below.

- Identify which measurements are important and can be included in the control system and how they should be implemented to lower signal variations and improve the disturbance rejection of the system.
- How much the energy consumption of the compressors can be lowered by obtaining less signal variations in the airflow.
- If the decreased signal variation gives a more favorable operating pattern of the compressors in terms of wear and tear.

1.3 Limitations

As the aim is to investigate the control and energy consumption of the aerators, which are located in the biological treatment step, it is therefore natural to only model this part of the treatment plant. All other treatment processes, such as filters and screens, will not be included in this study. In the modeled treatment processes, phosphorus will not be considered as the levels are much lower than those of nitrogen and organic material, and the treatment process is not directly connected to the latter two.

The Käppala WWTP has an old and new part. In this thesis only the new part is considered. It will also be assumed that the flow controllers and valves for air supply are ideal and they will therefore not be modeled. Limitations exist in what tests are possible to perform on the system, which limits the data collection and modeling. Some restrictions in data access might also appear, as well as difficulty in measuring certain parameters.

2

Theory

This section provides an understanding of the many processes that are part of wastewater treatment. This includes both the chemical compounds and reactions that are present in wastewater treatment as well as explanations of the relevant parts of the treatment plant and the biological, chemical and physical mechanisms that drive them. Lastly, the theory on the control strategies used for this thesis will be presented.

2.1 Constituents in wastewater

The wastewater treated in WWTP consists mainly of three large parts: nitrogen, phosphorus and organic material [3]. In addition, it also contains pathogens (such as bacteria and viruses), oil, grease and a large number of different chemicals that can have a high toxicity, for example solvents and pesticides to name a few. However, these will not be discussed further in this report as the focus is on the biological treatment, which has the main purpose of removing nitrogen and organic material. Phosphorus is also present and removed in the biological treatment, but the content is lower than that of nitrogen and organic material and will not be considered in this thesis. It will be seen as a parallel process that does not affect the system.

2.1.1 Organic material

The content of organic material is often measured as an aggregate of organic compounds [3]. Two of the most common are biochemical oxygen demand (BOD) and chemical oxygen demand (COD). BOD indicates the amount of oxygen used by microorganisms to break down organic material during a specified number of days, in Sweden normally seven (BOD_7). COD instead represents the oxygen needed to chemically oxidize the organic material using an oxidant, e.g. dichromate. However, because chrome is toxic, plants can also choose to measure total organic carbon (TOC) instead. It is measured by converting all organic material to carbon dioxide using either heat or chemicals. The carbon dioxide can then be used to calculate the value of COD.

Usually, COD is used as a measure of the organic material content. The composition of COD is described by the graph in Figure 2.1 and is divided into three major groups, which are then further divided [3]. Solubles are, as the name implies, parts that can be dissolved in water and the particulates are present as solids. Active

biomass is mainly bacteria and will be further described in Section 2.2. BOD is used to measure the biodegradable part of COD. The notation for the different components will be introduced in Section 4.1.1.

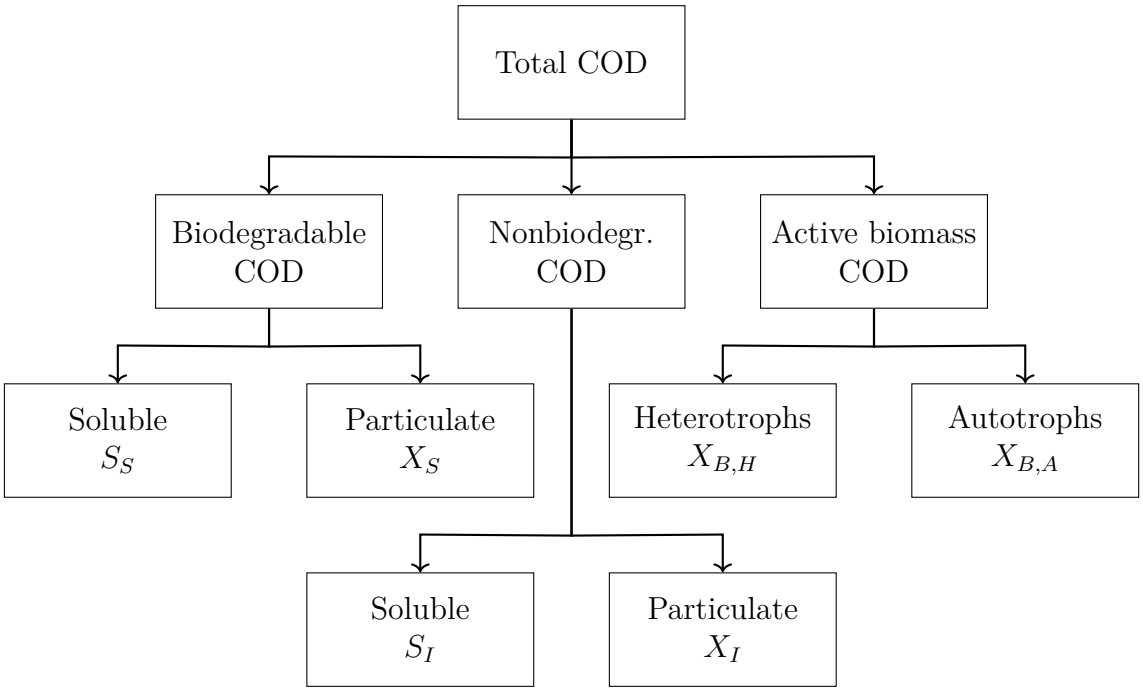

Figure 2.1: COD components with notation used in ASM1 model

2.1.2 Nitrogen

As with organic material, nitrogen in wastewater also takes different forms, such as ammonia, organically bound nitrogen and nitrate. These forms, among others, make up the total nitrogen (TN), shown in Figure 2.2 [3]. The notation is in line with the activated sludge model nr. 1 (ASM1) model used and will be described in further detail in Section 4.1.1. The largest share of nitrogen in wastewater is ammonium in the form of ions that are in equilibrium with free ammonium. Other forms include organically bound nitrogen, nitrogen contained within bacterial biomass (active biomass), and nitrogen in the form of nitrate and nitrite, where the latter two have very low concentrations in the incoming wastewater.

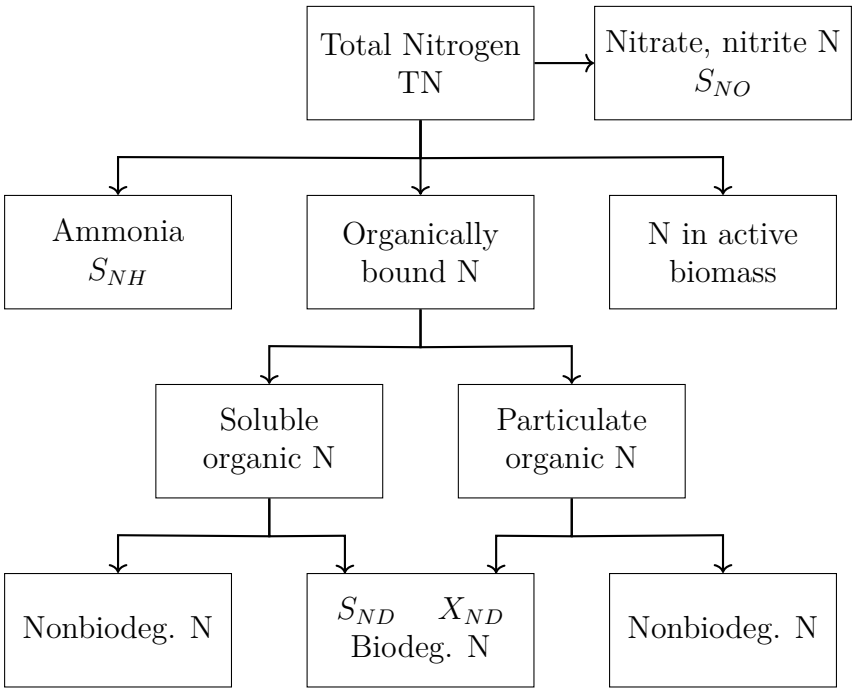

Figure 2.2: Composition of nitrogen content in influent wastewater.

2.2 Biological processes

The process of removing pollutants from wastewater with microorganisms is called the activated sludge process and is the most common method of secondary wastewater treatment (biological treatment) in the world [4]. As mentioned previously, the constituents discussed in this report will be nitrogen and organic material. These are removed by two major processes called nitrification and denitrification. These reactions are shown in Equations (2.1) and (2.2).

$$\begin{aligned} NH_4^+ + \frac{3}{2}O_2 &\rightarrow NO_2^- + H_2O + 2H^+ \\ NO_2^- + \frac{1}{2}\mathrm{O}_2 &\rightarrow NO_3^- \end{aligned} \tag{2.1}$$

$$4NO_3^- + 5"CH_2O" + 4H^+ \rightarrow 2N_2 + 7H_2O \tag{2.2}$$

where "CH_2O" represents organic matter of different types [5].

During the nitrification process, oxygen is required, as it is an oxidizing agent needed to convert ammonia into nitrate. This occurs in two steps of oxidation, as ammonia is initially converted to nitrite before reacting with oxygen to form nitrate, which is shown in Equation (2.2). Denitrification then converts the nitrate to nitrogen gas with organic material as the energy source and hence also serves as the organic

material removal. For denitrification, conditions with little or no dissolved oxygen with nitrate present are needed. These conditions are called anoxic conditions [4]. Nitrification is performed by autotrophic organisms in the presence of oxygen, while denitrification is performed by heterotrophic organisms with the use of nitrate as a respiratory substrate [5, 6].

2.3 Oxygen transfer

Oxygen plays a crucial role in the biological process, since treatment is done by microorganisms, which in turn require oxygen to metabolize. However, the nitrification reaction shown in Equation (2.1) is the largest oxygen demand. Oxygen is naturally transferred from gas to liquid through mass transport, but this phenomenon is very slow because of the small contact area between the air and the water, in addition to the volume of water. To accommodate for this, the area of transfer is increased by having bubbles from the aeration system travel through the basins. Modeling of the oxygen transfer from the bubbles to the water is governed by the oxygen transfer coefficient K_La. It represents the speed of mass transfer from a specified tank volume. The change in dissolved oxygen concentration, in the absence of organic matter and without inlet or outlet flow, can therefore be described as in equation (2.3) [7]:

$$\frac{dDO(t)}{dt} = K_La(DO_{sat} - DO(t)) \tag{2.3}$$

In equation (2.3) $DO(t)$ is the dissolved oxygen, DO_{sat} is the saturated oxygen concentration. The oxygen transfer rate has been shown to slow down as it approaches the saturation level [2]. The oxygen transfer function K_La is usually described as a nonlinear function because it needs to capture the saturated dynamics of the bubble transfer. Modeling this function can be a difficult task, as it is a nonlinear function, with respect to the airflow rate dependent on the geometry and operating conditions of the system, some of which are difficult to estimate, such as turbulence and bubble size [5]. The model for the K_La function is addressed in Section 4.1.1.1.

2.4 Aeration system

Oxygen is supplied to the water basins by either mechanical or diffused aerators [3]. Because diffused aerators are used at Käppala, only they will be considered. They work by blowing air into the basins at the bottom. The diffusers have very small holes and are distributed over the bottom of the basins to ensure that small air bubbles are equally distributed in the water volume. Smaller bubbles increase the transfer of oxygen from gas to water because the contact area relative to the volume is larger, which gives a better oxygen transfer. In addition, the bubbles also ensure good mixing in the basins.

The aerators in WWTPs, commonly referred to as blowers, are usually of the displacement or centrifugal type [2]. From the blowers, air is distributed to the different

basins in the WWTP. The modeling of compressors is based on a performance map, which describes the relationship between flow, discharge pressure and rpm.

2.5 Settler

Settlers are used throughout the water treatment process with a dual purpose: clarification and thickening. Settlers can be located throughout the plant, a primary settler is located before the system (outside the system borders) and secondary settlers are located after the biological treatment and help decrease the concentration of particulates in the effluent. The particulates accumulate at the bottom of the settler, where the thickened stream can be recirculated to recover the bacteria back into the biological treatment system. The settler works by letting gravity bring the heavier particulate components towards the bottom, leading to a concentration gradient in the tank. The soluble components can be treated as not affected by the thickening process, and thus the concentration of solubles is the same at the bottom as at the top of the settler [5].

2.6 Control theory

Industrial processes rarely operate autonomously, rather process control is almost always present. Designing controllers for a process can be done in many different ways, some of which will be explored in this thesis. The commonly used PID (and the different variants) control will be treated as assumed knowledge. Other methods are explored and the theory behind them is presented in this section.

2.6.1 Cascade

Cascade control is a fundamental concept in control theory. It describes the approach of utilizing two or more controllers in a hierarchical setup, where one controller sets the setpoint for another controller [8]. In a cascade control setup, it is important that the inner control loop is much faster than the outer control loops. This has multiple advantages, such as the inner loop having a linearizing effect on the outer loops as well as counteracting disturbances. An example of a simple cascade setup is shown in Figure 2.3.

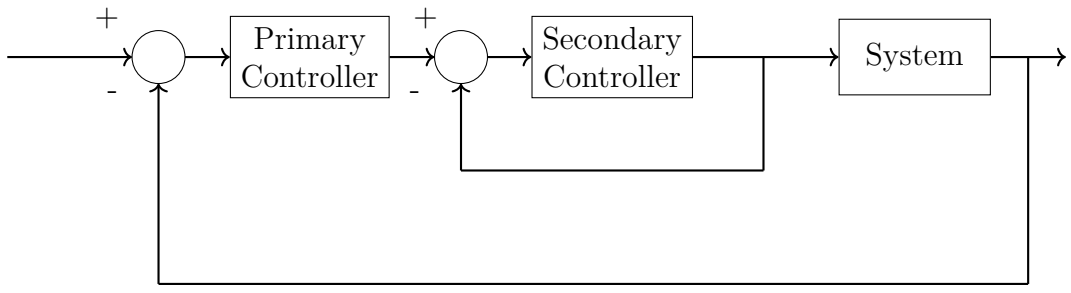

Figure 2.3: Cascade control with one inner and one outer loop.

2.6.2 Feedforward

The usual way to control a system is using feedback control. The controller uses the measured value in the system to adjust the input variable in order to reach the desired setpoints. Of course, this means that a change in the inflow properties of the system needs to propagate through the whole system before the controller can react. If the residence time (time constant) of the system is long, this can give a very long response time for the controller. One way to overcome this problem is to use what is called feedforward control in combination with the regular feedback controller [9]. It uses some measurement of an incoming variable (process disturbance) and makes it possible for the control system to react before any effect on the measured variable can be detected. A schematic drawing of a feedforward/feedback control system can be seen in Figure 2.4.

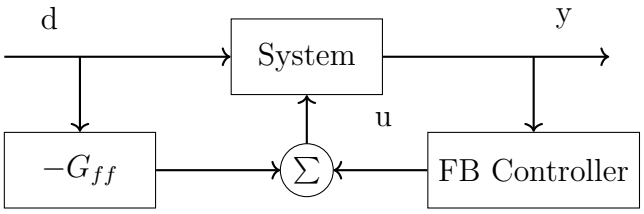

Figure 2.4: Schematic picture for feedforward control combined to feedback control.

A good starting point for designing a feedforward controller is the ideal feedforward compensator described by Equation (2.4), where G_{yd} and G_{yu} are the transfer functions from process disturbance and control signal respectively to the output signal [10].

$$G_{ff} = \frac{G_{yd}}{G_{yu}} \tag{2.4}$$

The feedforward will then be set as $-G_{ff}$ in order to counteract the disturbance.

2.6.3 Gain scheduling

Gain scheduling has historically been the most common way of controlling nonlinear systems [11]. It can be explained as switching between multiple linear controllers, tuned for the local description of the nonlinear system. The scheduling between these local controllers creates an overarching non-local controller. This is beneficial as a linear controller is usually only able to control the nonlinear system locally. The scheduling can be done in many different ways, usually by taking a measurement value and changing controller values when it exceeds or drops below a certain value. One of the main challenges with gain scheduling is the transition between values. It can cause a decrease in performance or even lead to instability, as the closed-loop behavior of the local controllers may vary significancy for different operating points [11].

2.6.4 Linear quadratic Gaussian (LQG)

A linear quadratic Gaussian (LQG) controller is a linear quadratic regulator (LQR) combined with a state observer [12]. It is a model-based controller that aims to take the system to its equilibrium points in the most effective way by minimizing a cost function. The estimator and controller will be described more closely in Section 2.6.4.3 and 2.6.4.4 after some foundation is established.

It is preferred to describe the system in the form of a state-space model to design an LQG controller. As most systems are not entirely linear, the differential equations describing the system in most cases need to be linearized before being put on state-space form. For a multiple input multiple output (MIMO) system, the state-space model is preferably put in matrix form for compact notation, presented in Equation (2.5).

$$\begin{aligned} \dot{x}(t) &= Ax(t) + Bu(t) + Nv(t) \\ y(t) &= Cx(t) + Du(t) + w \end{aligned} \tag{2.5}$$

In Equation (2.5) A is the state matrix, B is the input matrix, N the input noise matrix, x is the linearized state vector, u the control signal, v is process noise and w being measurement noise.

2.6.4.1 Controllability and stabilizability

The concept of controllability describes how the states are influenced by the input u [12]. A state is said to be controllable if there exists an input that can move the state from its initial value to its final value in a finite time. A system is controllable if this holds for all states. Even if the system is not controllable, it can still be stabilizable, meaning that the noncontrollable states do not cause instability. Naturally, a controllable system is always stabilizable.

2.6.4.2 Observability and detectability

The concept of observability describes how the internal states of the system can be inferred from the output [12]. A state is said to be observable if it is possible to determine its initial value from the knowledge of only the output. A system is observable if this holds for all states. Even if the system is not observable, it can still be detectable, meaning that the non-observable states do not cause instability. As with stabilizability, detectability also implies observability.

2.6.4.3 Optimal control feedback

Linear quadratic controllers/regulators (LQR) are designed to minimize the quadratic cost function in Equation (2.6).

$$J_{[0,\infty]} := \int_0^\infty x^T(t)Q_x x(t) + u^T(t)Q_u u(t)dt \tag{2.6}$$

In Equation (2.6), x(t) are the system states and u(t) are the control inputs. Q_u and Q_x are positive semi-defined matrices, which means that the matrices are symmetric and all eigenvalues are non-negative [13]. Given that the cost function is defined on an infinite horizon $[0, \infty]$, finding a solution that minimizes the cost function is best done by solving the algebraic Riccati equation (ARE) in Equation (2.7) [14].

$$0 = A^T P + PA - PBQ_u^{-1}B^T P + Q_x \tag{2.7}$$

P in Equation (2.7) is a symmetric unknown matrix with the same dimensions as A. By solving Equation (2.7) P can be used to find a solution for the optimal control gain K.

$$u(t) := -Q_u^{-1}B^T Px(t) = -Kx(t) \tag{2.8}$$

In Equation (2.8) a stabilizing solution to the problem is given as the linear state feedback gain, K[14].

2.6.4.4 Optimal state observer

To properly utilize the controller described in Equation (2.8), a state observer is typically needed because all states are rarely not observable. The state observer is typically a Kalman filter and the optimal linear state observer is of the form in Equation (2.9)

$$\dot{\hat{x}}(t) = A\hat{x}(t) + Bu(t) + L(y(t) - C\hat{x}(t)) \tag{2.9}$$

where

$$L := PC^T R^{-1} \tag{2.10}$$

and

$$P(t) = E\{(x(t) - \hat{x}(t))(x(t) - \hat{x}(t))^T\} \tag{2.11}$$

while satisfying the filter algebraic Riccati equation (FARE) in Equation (2.12)

$$0 = A^T P + PA - PC^T R^{-1}CP + Q \tag{2.12}$$

where Q and R are the covariance matrices for the disturbances v and w respectively[14].

Combining the regulator and the observer gives an LQG controller for which the structure can be seen in Figure 2.5.

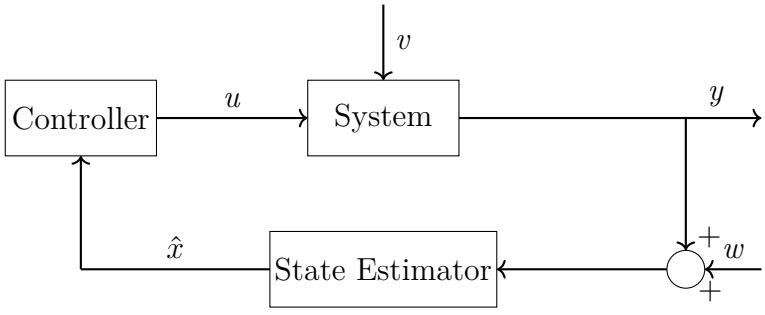

Figure 2.5: Block diagram for a general LQG structure.

The LQG solution is an offline solution meaning that it can be calculated ahead of time, both the controller and the model parameters it is based on are not time dependent.

3

System Description

Käppala, located on the island of Lidingö in Stockholm, is one of the largest municipal WWTPs in Sweden, treating wastewater from 11 municipalities [3]. The original plant was constructed in 1969. Since then, it has been expanded and is today divided into a new and an old section. Almost the entire WWTP is located underground.

3.1 General process description

The plant is divided into multiple lines, with lines 1-6 forming the old section and lines 7-11 comprising the new section [3]. The process layout of different lines is similar and the layout is seen in Figure 3.1. The main differences are differences in physical dimensions between the new and old parts together with the control systems being different between individual lines.

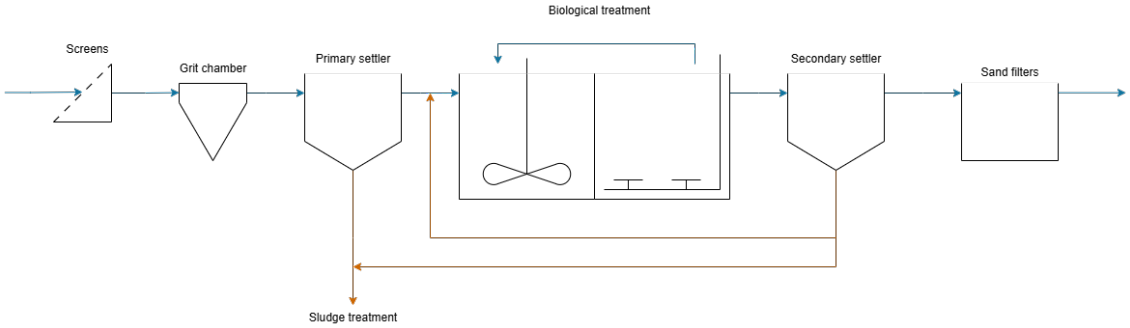

Figure 3.1: Process scheme, Käppala wastewater treatment plant.

The water flows from left to right in Figure 3.1. The first part of the process consists of screens, where larger objects, such as toilet paper, are separated from the stream. The screens are followed by a grit chamber that removes sand and gravel from the incoming wastewater [15]. To the right of the grit chamber, in Figure 3.1, the primary settler is located, where some larger particulate matter sinks to the bottom and is taken to the sludge treatment, where biogas is produced. The main part of the process is the biological treatment which is explained more in detail in Section 3.1.1. After the biological treatment, the secondary settler follows. Here, sludge is once again separated from the water but most of it is recirculated back into the biological treatment, as the sludge contains a lot of microorganisms. The rest is sent

to the same sludge treatment as the sludge from the primary settler [15]. Finally, the water is sent through sand filters before being released into the sea.

3.1.1 Biological treatment

In the biological treatment step, microorganisms are utilized to remove nitrogen in the form of ammonia from the wastewater [2]. This process occurs in two steps, nitrification and denitrification, where ammonia is converted to nitrogen gas with an intermediate step as nitrate. The first step is oxic, meaning that oxygen should be present. Therefore, oxygen is required for the bacteria to convert ammonia to nitrate. In the second step, during the conversion of nitrate to nitrogen, the bacteria needs anaerobic conditions (absence of oxygen) and consumes organic matter as an energy source. However, in the process, these two steps are put in the opposite order and there is a recirculation flow from the oxic part to the anaerobic part. It is done this way because the organic material needs to be oxidized in the nitrification before the bacteria in the denitrification can use it as energy.

3.2 Control structure

The control structure for the new part of the Käppala WWTP consists of a cascade control setup in three levels with PI regulators. The ammonium (NH) controller that controls the oxygen level setpoint for the basins. The oxygen level (DO) controller set the flow setpoint for the basins. Then, a flow controller adjusts the valve positions to maintain the right flow. The latter, together with the valve, has in this project been seen as ideal and therefore not modeled. The structure can be seen in Figure 3.2 showing the biological treatment basins and the secondary settler from Figure 3.1.

It is worth noting that the first DO controller uses the measurement from the first half of the second basin but controls the airflow to both that and the first basin.

The ammonium level is measured by a sensor placed after the secondary settler to avoid problems in maintaining the accuracy, as the sensor has a tendency to clog up with solid material [3]. Even then, there are still problems with the accuracy of the measurement. In [3], the sensor measurements were compared with samples analyzed in a laboratory. A noticeable drift of the sensor and the need for frequent recalibration was discovered, which means that the accuracy can be questionable in some cases also affecting the control system performance.

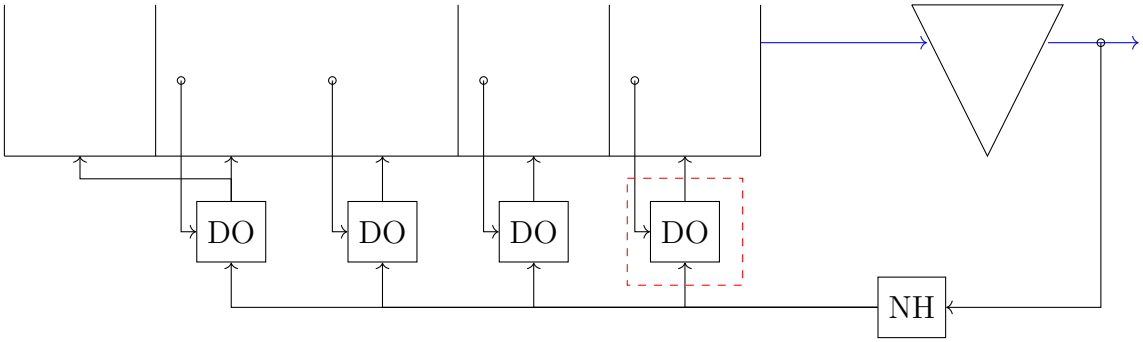

(a) Overview of ammonium and DO controllers. Details of the red dashed box are shown in (b).

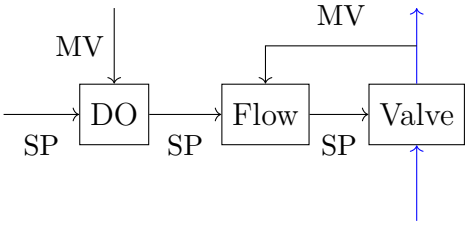

(b) Detailed scheme for the DO and flow controllers. SP denoting set point and MV denoting measurement value.

Figure 3.2: Control structure for the new part of the plant and lines 9-11 where ammonium feedback controllers are installed. For lines 7-8 the SP for the DO controllers are set manually.

4

Method

The method used for this thesis begins with modeling of the dynamic systems with the goal of accurately enough describing the system. With a sufficient model, control systems can much more easily be designed and evaluated. MATLAB and Simulink were used for the modeling and simulation. MATLAB was used to aid in the control system design, with tests done on the Simulink model, partially with real-world data provided by Käppala.

4.1 Modeling

Mathematical models have been used to describe the wastewater treatment system, primarily for the biological treatment and the post-settler, but also for the blower. The biological treatment part utilize the preexisting Activated sludge model NO.1 (ASM1) created by [16] described in detail below. The model used for the post-settler is the 1D model by [17]. All parameters, both general and plant specific, used can be found in Appendix A. For the blowers the model was based on the data sheet provided by the manufacturer.

Many studies use days as the unit of time when using the ASM1 model. In this thesis however, the choice was made to use hours instead. The reason for that being that many studies focus on long simulation horizons, one or several years and consequently the long term performance of the system. In this work, the focus instead has a time span of up to a couple of months with sudden changes spanning a maximum of 2-3 days. Therefore, in order to make sure that the data has adequate time resolution and to make it more understandable the change was made.

4.1.1 ASM1

The biological processes in a WWTP are difficult to model, but there exists multiple ways to do it. The most commonly used model is the Activated Sludge Model no. 1 [5] developed in 1987. It utilizes Monod equations [18] to describe the parallel processes occurring in the aerobic tanks [16]. The processes describing the biological system are as follows: removal of organic matter, nitrification and denitrification. It results in 13 coupled states, some of which can be removed to help simplify the system, these include alkalinity, particulate products and inert components. This leads to a reduction of states, with 9 states remaining. The set of ODEs describing the system is provided in Equations (4.1a) - (4.1i) and the states are given in Table

4.1.

Table 4.1: Concentrations (states) for the ASM1 model. Particulates are denoted X and solubles are denoted S

S_S	Readily biodegradable substrate
X_S	Slowly biodegradable substrate
$X_{B,H}$	Active heterotrophic biomass
$X_{B,A}$	Active autotrophic biomass
DO	Dissolved oxygen
S_{NO}	Nitrate and nitrite nitrogen
S_{NH}	$NH_4^+ + NH_3$ nitrogen
S_{ND}	Soluble biodegradable organic nitrogen
X_{ND}	Particulate biodegradable organic nitrogen

The differential equations used to describe the evolution of states are described in Equations (4.1a)-(4.1i).

$$\begin{aligned}\frac{dS_S(t)}{dt} =& \frac{Q}{V}(S_{S,in} - S_S(t)) - \frac{1}{Y_H}\mu_{max,H}\left(\frac{S_S(t)}{K_S + S_S(t)}\right)\left(\frac{DO(t)}{K_{O,H} + DO(t)}\right)X_{B,H}(t) \\ &- \frac{1}{Y_H}\mu_{max,H}\left(\frac{S_S(t)}{K_S + S_S(t)}\right)\left(\frac{K_{O,H}}{K_{O,H} + DO(t)}\right)\left(\frac{S_{NO}(t)}{K_{NO} + S_{NO}(t)}\right)\eta_g X_{B,H}(t) \\ &+ k_h \frac{\frac{X_S(t)}{X_{B,H}(t)}}{K_X + \frac{X_S(t)}{X_{B,H}(t)}}\left(\left(\frac{DO(t)}{K_{O,H} + DO(t)}\right) + \eta_h\left(\frac{K_{O,H}}{K_{O,H} + DO(t)}\right)\left(\frac{S_{NO}(t)}{K_{NO} + S_{NO}(t)}\right)\right)X_{B,H}(t)\end{aligned} \tag{4.1a}$$

$$\begin{aligned}\frac{dX_S(t)}{dt} =& \frac{Q}{V}(X_{S,in} - X_S(t)) + (1 - f_p)(b_H * X_{B,H}(t) + b_A X_{B,A}(t)) \\ &- k_h k_{sat}\left(\left(\frac{DO(t)}{K_{O,H} + DO(t)}\right) + \eta_h\left(\frac{K_{O,H}}{K_{O,H} + DO(t)}\right)\left(\frac{S_{NO}(t)}{K_{NO} + S_{NO}(t)}\right)\right)X_{B,H}(t)\end{aligned} \tag{4.1b}$$

$$\begin{aligned}\frac{dX_{B,H}(t)}{dt} =& \frac{Q}{V}(X_{B,H,in} - X_{B,H}(t)) + \mu_{max,H}\left(\frac{S_S(t)}{K_S + S_S(t)}\right)\left(\frac{DO(t)}{K_{O,H} + DO(t)}\right)X_{B,H}(t) \\ &+ \mu_{max,H}\left(\frac{S_S(t)}{K_S + S_S(t)}\right)\left(\frac{K_{O,H}}{K_{O,H} + DO(t)}\right)\left(\frac{S_{NO}(t)}{K_{NO} + S_{NO}(t)}\right)\eta_g X_{B,H}(t) - b_H X_{B,H}(t)\end{aligned} \tag{4.1c}$$

$$\begin{aligned}\frac{dX_{B,A}(t)}{dt} =& \frac{Q}{V}(X_{B,A,in} - X_{B,A}(t)) + \mu_{max,A}\left(\frac{S_{NH}(t)}{K_{NH} + S_{NH}(t)}\right)\left(\frac{DO(t)}{K_{O,A} + DO(t)}\right)X_{B,A}(t) \\ &- b_A X_{B,A}(t)\end{aligned} \tag{4.1d}$$

$$\begin{aligned}\frac{dDO(t)}{dt} =& \frac{Q}{V}(DO_{in} - DO) + K_L a(DO_{sat} - DO(t)) \\ &- \frac{1 - Y_H}{Y_H}\mu_{max,H}\left(\frac{S_S(t)}{K_S + S_S(t)}\right)\left(\frac{DO(t)}{K_{O,H} + DO(t)}\right)X_{B,H}(t) \\ &- \frac{4.57 - Y_H}{Y_H}\mu_{max,A}\left(\frac{S_{NH}(t)}{K_{NH} + S_{NH}(t)}\right)\left(\frac{DO(t)}{K_{O,A} + DO(t)}\right)X_{B,A}(t)\end{aligned} \tag{4.1e}$$

$$\begin{aligned}\frac{dS_{NO}(t)}{dt} =& \frac{Q}{V}(S_{NO,in} - S_{NO}(t)) - \frac{1 - Y_H}{2.86Y_H}\mu_{max,H}\left(\frac{S_S(t)}{K_S + S_S(t)}\right)\left(\frac{K_{O,H}}{K_{O,H} + DO(t)}\right)\left(\frac{S_{NO}(t)}{K_{NO} + S_{NO}(t)}\right)\eta_g X_{B,H}(t) \\ &+ \frac{1}{Y_A}\mu_{max,A}\left(\frac{S_{NH}(t)}{K_{NH} + S_{NH}(t)}\right)\left(\frac{K_{O,A}}{K_{O,H} + DO(t)}\right)X_{B,A}(t)\end{aligned} \tag{4.1f}$$

$$\begin{aligned}\frac{dS_{NH}(t)}{dt} =& \frac{Q}{V}(S_{NH,in} - S_{NH}(t)) - i_{X,B}\mu_{max,H}\left(\frac{S_S(t)}{K_S + S_S(t)}\right) \\ & \cdot \left(\left(\frac{DO(t)}{K_{O,H} + DO(t)}\right) + \left(\frac{K_{O,H}}{K_{O,H} + DO(t)}\right)\left(\frac{S_{NO}(t)}{K_{NO} + S_{NO}(t)}\right)\eta_g\right) X_{B,H}(t) \\ & - \left(i_{X,B} + \frac{1}{Y_A}\right)\mu_{max,A}\left(\frac{S_{NH}(t)}{K_{NH} + S_{NH}(t)}\right)\left(\frac{DO(t)}{K_{O,A} + DO(t)}\right) X_{B,A}(t) + k_A S_{ND}(t) X_{B,H}(t)\end{aligned} \tag{4.1g}$$

$$\begin{aligned}\frac{dS_{ND}(t)}{dt} =& \frac{Q}{V}(S_{ND,in} - S_{ND}(t)) - k_A S_{ND}(t) X_{B,H}(t) \\ & + k_h k_{sat}\left(\left(\frac{DO(t)}{K_{O,H} + DO(t)}\right) + \eta_h\left(\frac{K_{O,H}}{K_{O,H} + DO(t)}\right)\left(\frac{S_{NO}(t)}{K_{NO} + S_{NO}(t)}\right)\right) X_{B,H}(t)\frac{X_{ND}(t)}{X_S(t)}\end{aligned} \tag{4.1h}$$

$$\begin{aligned}\frac{dX_{ND}(t)}{dt} =& \frac{Q}{V}(X_{ND,in} - X_{ND}(t)) + (i_{XB} - f_P i_{XP})(b_H X_{B,H}(t) + b_A X_{B,A}(t)) \\ & - k_h k_{sat}\left(\left(\frac{DO(t)}{K_{O,H} + DO(t)}\right) + \eta_h\left(\frac{K_{O,H}}{K_{O,H} + DO(t)}\right)\left(\frac{S_{NO}(t)}{K_{NO} + S_{NO}(t)}\right)\right) X_{B,H}(t)\frac{X_{ND}(t)}{X_S(t)}\end{aligned} \tag{4.1i}$$

The parameters used in the ASM1 equations, in Equations (4.1a) - (4.1i) is defined in Appendix A. Multiple Monod expressions, a type of rate expressions used for bacterial growth, are used to model rate dependencies on several substrates, which is expressed in Equations (4.1a) - (4.1i). The ASM1 model comes with assumptions, some addressed in later models such as ASM2, ASM2d, ASM3 [19]. These assumptions are summarized below [16].

A1 The system operates at constant temperature.

A2 The pH is constant and near neutrality.

A3 No change in the nature of the organic matter.

A4 No effects of limitations of nitrogen, phosphorus and other inorganic nutrients.

A5 The correction factors η_g and η_h are fixed and constant.

A6 The coefficients for nitrification are assumed to be constant.

A7 The heterotrophic biomass is homogeneous and does not change with time.

A8 The entrapment of particulate organic matter in the biomass is assumed to be instantaneous.

A9 Hydrolysis of organic matter and organic nitrogen are coupled and occur simultaneously with equal rates.

A10 The type fo electron acceptors present does not affect the loss of active biomass by decay.

Despite these assumptions ASM1 is still widely used today as it often captures the dynamics in a municipal wastewater system well enough. Therefore, it was used to model the dynamics of the biological system in this project as well.

4.1.1.1 Oxygen transfer model

Unlike the ASM1 parameters, the K_La function is a facility-specific function. It depends on several factors, as mentioned in Section 2.3. The model chosen is a fine bubble diffuser model, where K_La is a function of the superficial gas velocity.

$$\begin{aligned} K_La &= C \cdot U_{SG}^{Y} \\ C &= k_1 \cdot DD^{0.25} + k_2 \\ U_{SG} &= \frac{Q_L}{\textit{Diffuser area}} \end{aligned} \tag{4.2}$$

where DD is the diffuser density, k_1 and k_2 are model parameters, Y is the exponential factor and U_{SG} is the specific air flow [20]. Values for the oxygen transfer model were chosen from a previous study on the same facility [3].

4.1.1.2 ASM1 extensions

Another reason for the continued use of the ASM1 model is that it can be modified and built upon. The modifications usually aim to remove or lessen one of the assumptions presented in Section 4.1.1. The first assumption mentioned is the premise that the system operates at a constant temperature, which naturally is not the case in reality. The effect of temperature on the ASM1 model is addressed by allowing the rates vary with temperature. This change is presented in Equation (4.3) [21].

$$k_i(T) = k_{i,15°C} \cdot e^{\theta_i(T-15)} \tag{4.3}$$

where $k_{15°C}$ is the parameter value at $15°C$ and θ_i is the temperature correction factor. This correction is applied to the growth and decay coefficients in the ASM1 model since they are most affected by changes in water temperature [21].

The important oxygen transfer coefficient, K_La is also temperature dependent. Its temperature dependency is expressed by an Arrhenius function [2]. It is shown in Equation (4.4).

$$K_La(T) = K_La_{15°C} \cdot \theta^{15-T} \tag{4.4}$$

The correction factors for the different rates are given in Table A.2. These factors are used to recalculate the temperature dependent coefficients to their values at 15°C, because the ASM1 parameters found in Table A.4 are given at that temperature. It is assumed that the temperature corrections in Equation (4.3) and (4.4) hold for all plausible temperature disturbances that the system might experience.

Modifications are also made to the oxygen transfer rate described in Section 2.3. Because it is defined for pure water, while the model is of a WWTP, where the water is full of constituents as described in Section 2.1.1. To compensate, two correction factors are used, alpha (α) and beta (β), which are established in Equations (4.5) and (4.6).

$$\alpha = \frac{K_La \text{ (wastewater)}}{K_La \text{ (clean water)}} \tag{4.5}$$

$$\beta = \frac{DO_{sat} \text{ (wastewater)}}{DO_{sat} \text{ (clean water)}} \tag{4.6}$$

The correction factors α and β are used to calibrate K_La and DO_{sat} respectively, for wastewater, which can be seen by rearranging the expressions i Equations (4.5) and (4.6). The DO_{sat} in itself is a temperature dependent parameter. It was modeled with Equation (4.7) [22].

$$DO_{sat} = 14.3 - 0.411T + 9.6 \cdot 10^{-3}T^2 - 1.2 \cdot 10^{-4}T^3 \tag{4.7}$$

In Equation 4.7, T is the temperature in degrees Celsius. Values for important modeling parameters are presented in Appendix A.

4.1.2 Post settler

The post settler is located after the biological plant, as described in Figure 3.1. The settler model is done using [17] 1D model. The dynamics describing the system is represented in Figure 4.1 and Equations (4.8) - (4.12). The model divides the settling tank into multiple layers along the depth of the settling tank.

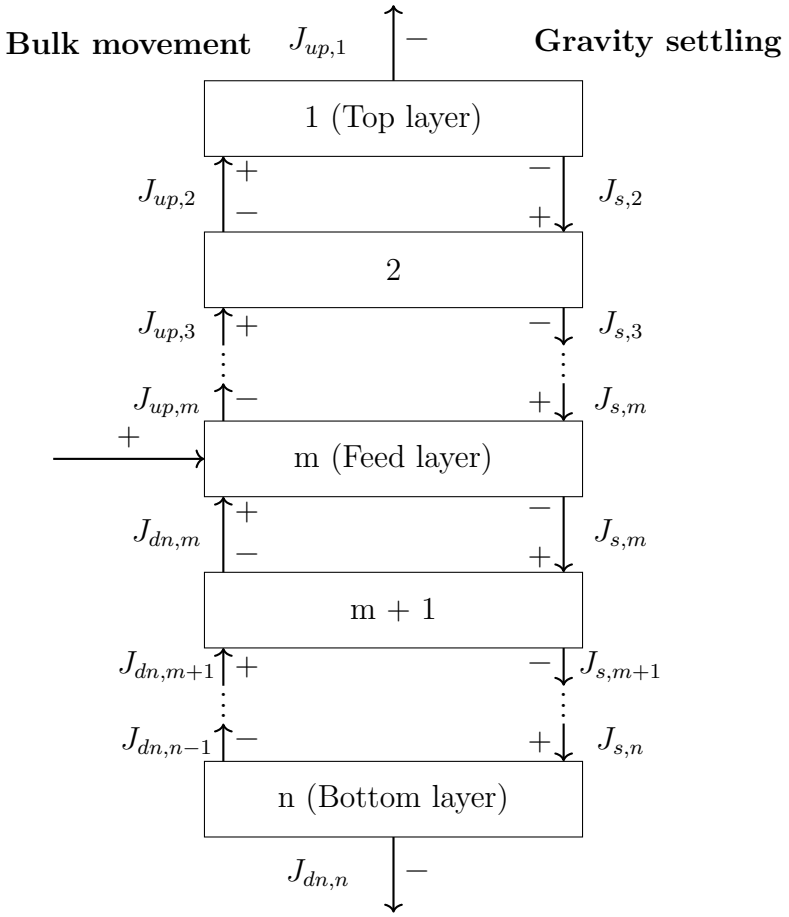

Figure 4.1: Balance of solids across the settler layers.

The settling velocity is calculated with the expressions in Equation (4.8).

$$\begin{aligned} v_{s,i} &= v_0 e^{-r_h(X_i - X_{min})} - v_0 e^{-r_p(X_i - X_{min})} \qquad 1 \leq i \leq n \\ 0 &\leq v_{s,i} \leq v_0' \end{aligned} \tag{4.8}$$

In Equation (4.8) v_s is the settling velocity, r_h and r_p are settling velocities. X_{min} is the minimum attained suspended solids concentration in the the effluent, calculated in Equation (4.9).

$$X_{min} = f_{ns} X_{in} \tag{4.9}$$

In Equation (4.9) f_{ns} is the non-settleable fraction and X_{in} the inlet concentration of particulates. The upwards and downwards fluxes can then be calculated as described in Equation (4.10).

$$\begin{aligned} J_{up,i} &= \frac{(Q_{in} - Q_w)X_i}{A} \\ J_{dn,i} &= \frac{(Q_{in} + Q_w)X_i}{A} \end{aligned} \tag{4.10}$$

Where J_{up} and J_{dn} is the material flux of the bulk movement above and below the inlet flow respectively. Q_{in} and Q_w is the is the inlet flow and waste flow respectively. A is the segment area (same as the basin surface area). The downwards material flux in the gravitational settling is denoted J_s and is calculated with Equation (4.11).

$$\begin{aligned} J_{s,i} &= \begin{cases} v_{s,i}X_i, & \text{if } X_i \leq X_t, \\ \min\Big(v_{s,i}X_i,\, v_{s,i+1}X_{i+1}\Big), & \text{if } X_i > X_t, \end{cases} \qquad \text{for } 1 \leq i < m, \\ J_{s,i} &= \min\Big(v_{s,i}X_i,\, v_{s,i+1}X_{i+1}\Big) \qquad \text{for } m \leq i \leq n-1. \end{aligned} \tag{4.11}$$

In Equation (4.11) $v_{s,i}$ is the settling velocity for that layer and X_i is the concentration of particulates in that layer. With the the downwards flux J_s defined the change in particulate concentration can be defined with Equation (4.12).

$$\begin{aligned} \frac{dX_1}{dt} &= \frac{1}{h}(J_{up,2} - J_{up,1} - J_{s,1}) \\ \frac{dX_i}{dt} &= \frac{1}{h}(J_{up,i+1} - J_{up,i} + J_{s,i-1} - J_{s,i}) \qquad 2 \leq i < m \\ \frac{dX_m}{dt} &= \frac{1}{h}(\frac{(Q_{in} + Q_s)X_{in}}{A} - J_{up,m} - J_{dn,m} + J_{s,m-1} - J_{s,m}) \\ \frac{dX_j}{dt} &= \frac{1}{h}(J_{dn,j-1} - J_{dn,j} + J_{s,j-1} - J_{s,j}) \qquad m+1 \leq i < n \\ \frac{dX_n}{dt} &= \frac{1}{h}(J_{dn,n-1} - J_{dn,n} + J_{s,n-1}) \end{aligned} \tag{4.12}$$

The evolution of the non-soluble concentrations in the settler layers is calculated with the help of the fluxes given in Equation (4.10) and Equation (4.11) as well as

the height of each layer, h and the inflow of particulates calculated from the inlet flow Q_{in} and the recycle flow Q_s. With differential equations defined in Equation (4.12) the evolution of the states, the particulate concentrations in each layer of the settler can be updated over time. The bottom concentration X_n is the concentration of the recycled flow. The concentration at the top layer is the concentration of the effluent flow. The change in soluble components is defined by a mass balance over the settler tank

$$\frac{dS_i(t)}{dt} = \frac{Q_{in}}{V}(S_i(t) - S_{i,in}(t)) \tag{4.13}$$

where $S_i(t)$ is a soluble component and $S_{i,in}$ is the input concentration of the same soluble.

4.1.3 Blower

For the blower model, a centrifugal compressor with the performance specified in Figure 4.2 is used. The data used for drawing the performance chart was provided by Käppala for one of their two stage blowers. It has two operating regions: the leftcorresponding to single-stage operations and the right to two-stage operations. As mentioned in Section 3.2 the valve characteristics has been omitted in this thesis. The valve will dynamically affect the pressure in the air supply line when changing the opening position. These pressure variations will therefore not be considered and the choice was made to evaluate the blower at the constant discharge pressure at the operating line. This is marked with red crosses in the compressor performance chart in Figure 4.2.

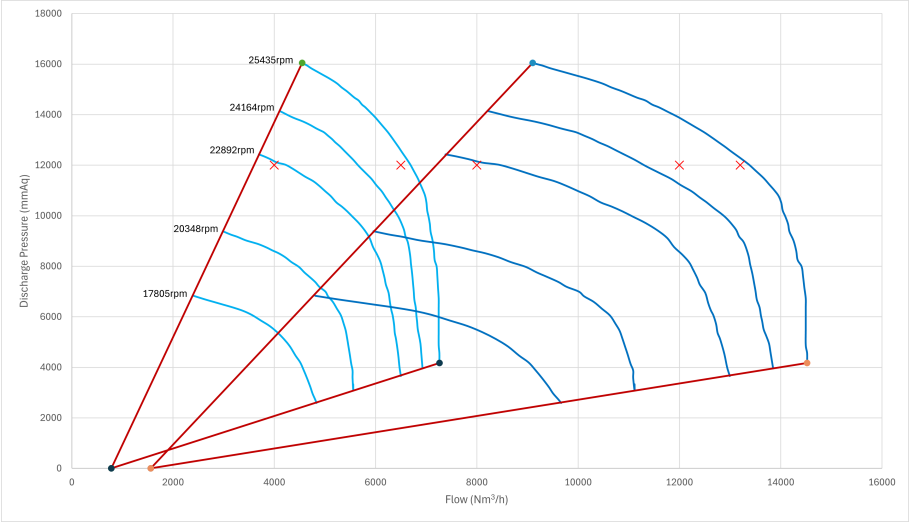

Figure 4.2: Compressor preformance chart

It can be concluded from the figure that the relation between flow and power is very close to linear and therefore a linear regression is performed to find that relation. The result of this is shown in Equation (4.14) which was used in the model to describe the power consumption of the compressor. The realistic behavior that larger changes in airflow can result in that a new blower needs to be started or turned off to

accommodate for the changes in required airflow is disregarded, instead all of the blowers are treated as one entity.

$$P(kW) = 0.0359 \cdot Q(Nm^3/h) - 1.4742 \tag{4.14}$$

4.2 Model validation

Model validation was performed by comparing output results of simulations with real-world data. The inputs given to the model for a specific time period were taken from real-world data. The inflow concentrations are not available as online measurements, but rather as weekly samples and were therefore interpolated for the input to the model. The control system was run in a setup as close to the real-world as possible but it was not possible to fully replicate this as it is unknown which controllers were run in auto or manual mode. Therefore, a guess of the setup was made based on the data available. Time periods were chosen to be relatively stable beginning with a sudden large transient in the inlet flow rate which also means transients in other inflow characteristics.

The importance of the model behaving exactly as the real system is not that great. It is however important that the dynamics of the system is captured by the model, especially in the situations where problematic behavior is exhibited. Therefore, no measurement of the model accuracy were used. The general dynamic behavior was compared to the real-world data and an assessment was made on how the model behavior compared to the real-world system.

Validation of the model created in Simulink is difficult because of the limited access to the internal states. States that can be observed in the model but are not measured in the real system. Thus, the model might initial seem to represent the plant well, but because of the hidden states, it can still be a faulty model. Furthermore, the system data is very noisy and complex, making it difficult to judge the cause and effect of the observed behaviors.

Taking the above into consideration, comparison between simulation and real-world data was only performed visually. It was noted how the simulation differed, primarily in its dynamic behavior, when comparing the graphs. It was also made sure that the total airflow to the system was reasonable comparable to the real world. This is important as the energy consumption is directly related to the airflow.

4.3 Control design

Given a validated, sufficiently good model, control design can be done. Especially in the case with WWTP:s because of the long time constants previously mentioned the risk exists that the inflow conditions change before for example a step response has been performed. This section presents how the control design for the three new schemes were made.

4.3.1 Feedforward control

The feedforward compensator was implemented by adding its signal to the existing NH controller seen in Figure 3.2a. In order to find the ideal feedforward compensator in Equation (2.4) step response analysis was used. As the transfer functions from both disturbance and control signal were needed, step responses for both of them were utilized in control design. The disturbances selected for feedforward compensation were inlet flow rate and inlet temperature as these are already measured accurately and are available. From the step responses, transfer functions from these disturbances and the input signal were found. With these one feedforward compensator for the inlet flow rate and one for the inlet temperature were constructed. These were tested on the step for which they were designed and then tuned to obtain a better performance.

4.3.2 LQG methodology

The linear state space model was created in MATLAB from the differential ASM1 equations for the tanks. Thus resulting in 82 states (changes in concentrations), 4 control inputs (air flows), 11 model disturbances (Inlet concentrations, inlet flow rate and inlet temperature) and 5 measured states (DO concentrations in aerated tanks and Ammonium effluent concentration). This abundance of states commonly arises in physical models, which proved to be the case for the WWTP model, described in Section 4.1. The MATLAB model is then used to create a linear state space model. Utilization built in MATLAB commands from the *Control Systems Toolbox*, both the controller and Kalman filter can be synthesized with the Matlab functions *lqr()* and *lqe()* respectively. The LQG synthetization is typically followed by rigorous tuning, but due to the results obtained in Section 5.2 this was not relevant.

4.3.3 Gain scheduling

A gain scheduled approach was investigated. It is based on the current PI ammonium feedback controller described in Section 3.2. By first deciding under which circumstances the model changes enough to justify a change in control gain. The system was, under constant DO set point, exposed to a series of steps in three different disturbances, inlet ammonium concentration, temperature and inlet flow with the DO kept constant. Steps in the inlet ammonium concentration showed very limited effect on the system. Both inlet flow and wastewater temperature were shown to have an effect on the system of similar magnitude, when exposing the system to disturbances of realistic size. Temperature was chosen as the preferred signal to schedule on, as it is an available and accurate measurement.

Two different operating conditions were chosen for the gain scheduling: one for lower temperature ($9^{\circ}C$) and one for warmer operating conditions ($15^{\circ}C$). The temperature measurement used should be one at the inlet as it serves as a feedforward signal forewarning the controllers. The system, under cold and warm operating conditions respectively response to the same step but under the different temperatures is presented below is Figure 4.3

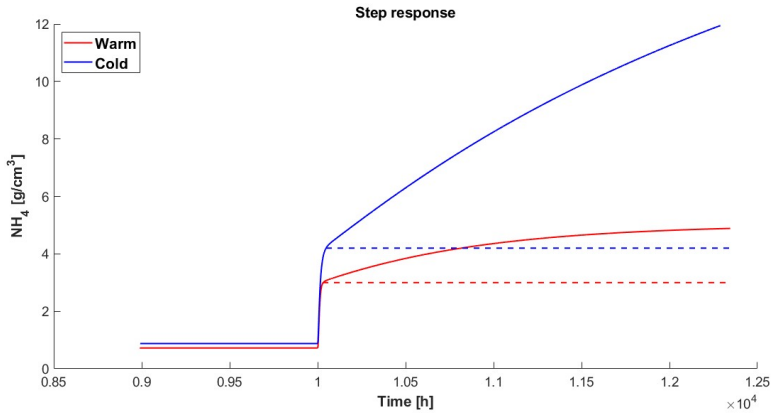

Figure 4.3: Effluent ammonium concentration step response for different temperatures

Based on similar step responses as the ones shown in Figure 4.3, two new PI controllers were designed and tuned with the Lambda method described in [23]. For that, the static gain (K_s) of the process must be calculated according to Equation (4.15). The time constant (τ) of the system and the dead time (T_d) should also be extracted from the step responses.

$$K_s = \frac{\Delta Y}{\Delta U} \tag{4.15}$$

In Equation (4.15), ΔY and ΔU are the changes in output and input, respectively. The control gain (K) and the integral time (T_i) can then be calculated from Equation (4.16).

$$K = \frac{\tau}{K_s(\lambda + T_d)} \quad T_i = \tau \tag{4.16}$$

Equation (4.16) utilizes the tuning parameter λ as well as the dead time T_d and the time constant τ.

A short algorithm was also developed to schedule the controllers, which is shown in pseudo-code in Algorithm 1.

Algorithm 1 Gain scheduling

```
new mode = current mode
if current mode = cold then
  if T > 13 then
    new mode = warm
  end if
else
  if T < 11 then
    new mode = cold
  end if
end if
Return new mode
```

Avoid rapidly swapping between the controllers at a crossover temperature is important, as that can in worst-case scenarios lead to instability. Therefore the controllers are scheduled in an overlapping way with different crossover temperatures, $11°C$ and $13°C$ respectively as can be seen in Algorithm 1.

4.4 Control system evaluation

The performance of the control strategies was evaluated in two main ways, graphical comparison of outgoing NH concentration and comparison of the energy consumption. The graphical comparison was made between each new control strategy and the existing one. The energy consumption for the different solutions was calculated as described in Section 4.1.3 and compared to the existing system. In all cases, the same setup of real world input data was used as for the model validation. In addition, a comparison was also made between new and existing control strategies of the DO setpoint and the total airflow but only for the feedforward of inlet flow rate.

5

Results

The results below demonstrate the validation of the model developed, by comparing its performance with real-world data. The result also contains the performance of the different control strategies developed in Section 4. This is also done by utilizing real-world data from Käppala WWTP. Energy consumption tables and graphs are presented that show this performance.

5.1 Model validation

Following the validation strategy described in Section 4.2, the following results were obtained. Figure 5.1 shows the comparison between the outgoing NH concentration in the outlet of the real system and the model during a time period from October 2020 to March 2021.

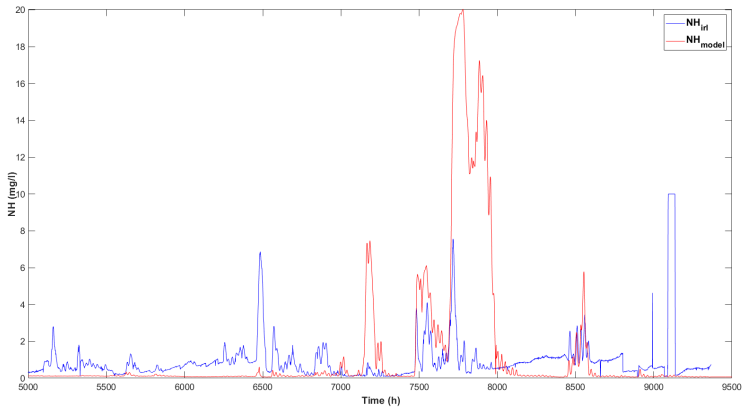

Figure 5.1: NH concentration in outflow for the period oct 2020 to mar 2021.

For the same time period, Figure 5.2 shows the DO in the aerated basins compared between the model and the real system.

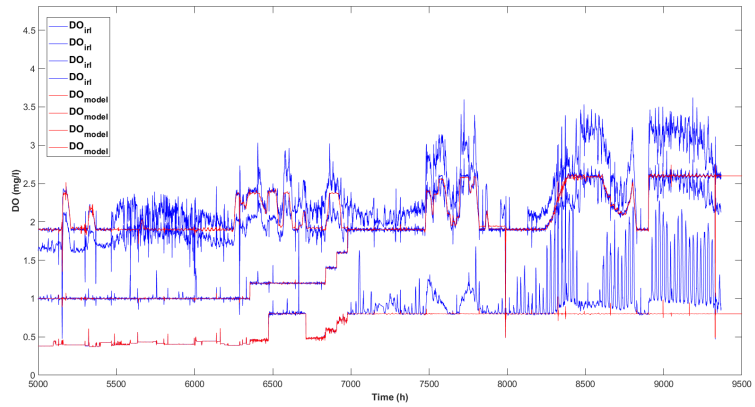

Figure 5.2: DO in the aerated basins for the period oct 2020 to mar 2021.

Figure 5.3 displays the total airflow comparison between the model and real system, also for the same time period as the previous two figures.

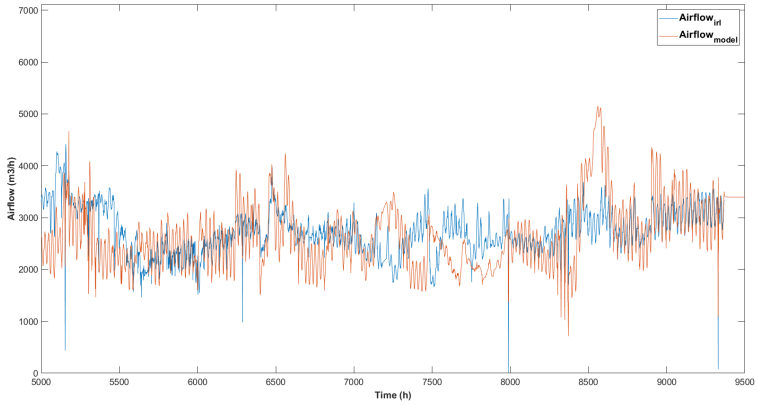

Figure 5.3: Total airflow for the period oct 2020 to mar 2021.

The same results were also obtained for the time period from September to December 2022. Figure 5.4 shows the outgoing NH concentration for the model compared to the real system during that time period.

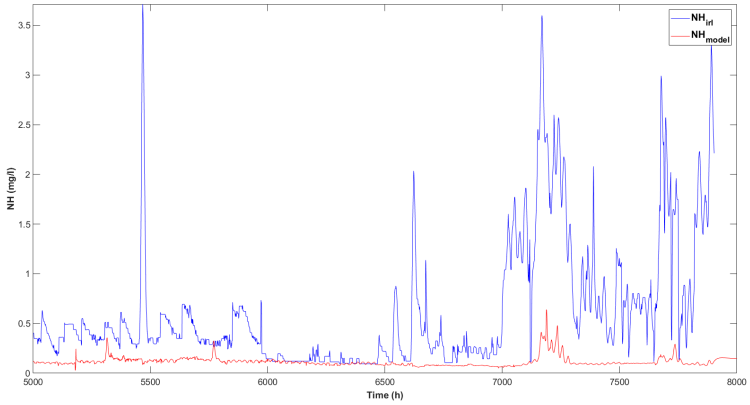

Figure 5.4: NH concentration in outflow for the period sep to dec 2022.

In Figure 5.5 the DO is instead compared during the same time period.

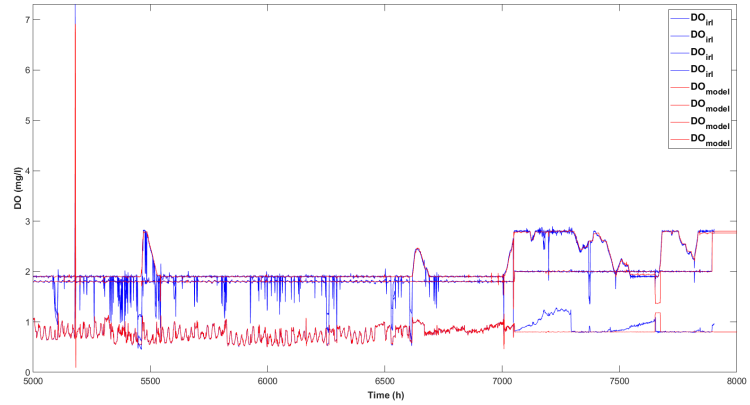

Figure 5.5: DO in the aerated basins for the period sep to dec 2022.

The total airflow is also compared between the model and the real system for the 2022 time period. The result can be seen in Figure 5.6.

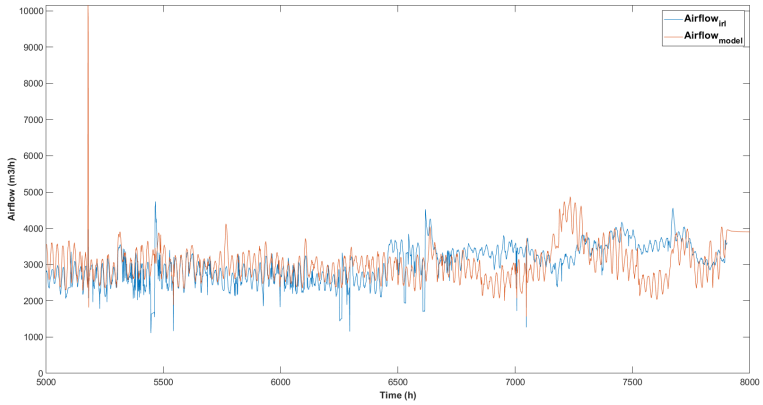

Figure 5.6: Total airflow for the period sep to dec 2022.

The model demonstrates stable behavior. However, the stability is only local, unstable regions exists outside of the regular operating region. Thus, making the system locally stable, not globally stable. The instability is presented further in Section 5.7.

5.2 LQG

The result for the LQG solution presented in Section 4.3.2. It can be concluded that linearizing the system around the operating point obtained from the existing ammonium-based feedback controller results in a controller that is unable to properly control the system. Instead, it diverges quickly when exposed to small deviations from the equilibrium. The results of simulating the nonlinear system alongside the linear system is shown in Figure 5.7. For practical reasons only the first six states are displayed. It can also be noted that the linearized model is neither observable nor controllable.

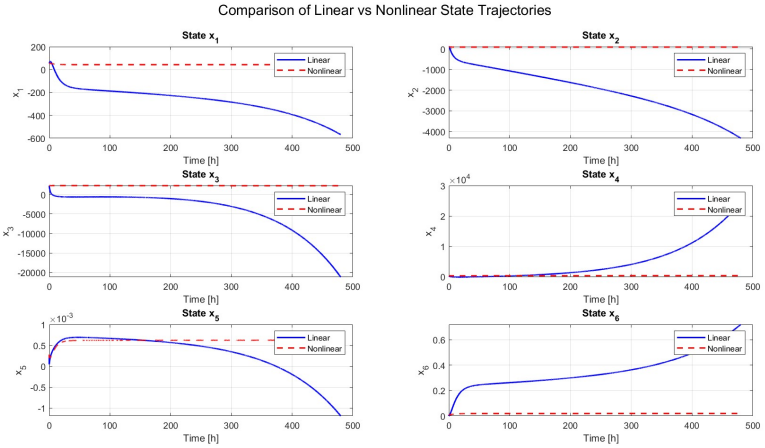

Figure 5.7: Simulation of the nonlinear and linear systems simultaneously showing the first six states.

Note that not only does the linearized model only approximate the nonlinear model in a very small region. It is also unstable and diverges. Result from simulating the the system without the post settler and instead with a simple recirculation is presented in Figure 5.8. Exactly like in the previous figure only the first six states are presented.

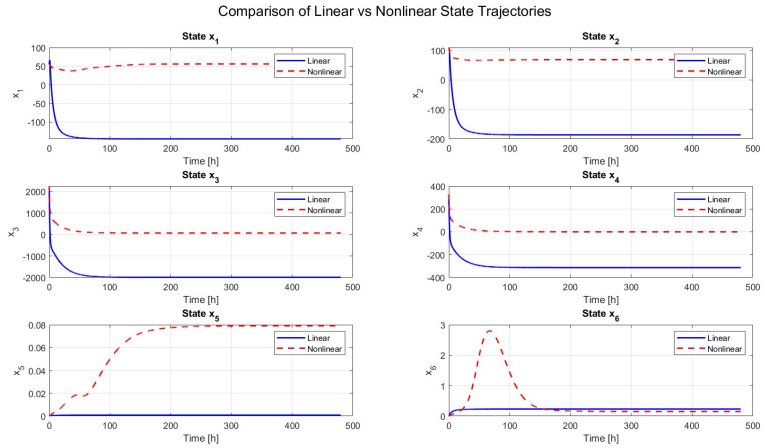

Figure 5.8: Simulation of the nonlinear and linear systems simultaneously without the settler showing the first six states.

Without the post settler it is stable but poorly approximated by the linear model which is shown in Figure 5.8. Like the unstable model in Figure 5.7, it is only accurate in a small region. However, it does not become unstable.

5.3 Gain scheduling

The gain scheduled solution consists of two synthesized and tuned ammonium feedback controllers on a scheduling. The scheduling being described in pseudo-code in Algorithm 1. The synthesis of which is described in Section 4.3.3, resulting in two controllers denoted *cold* and *warm* respectively. Their parameters can be seen in Table 5.1.

Table 5.1: Control parameters for the two controllers.

	K	T_i
cold	0.00288	19.40
warm	0.00379	16.00

Simulating the same two periods as for the feedforward control the graphs in Figures 5.9 and 5.10 show the outgoing ammonium concentration for the gain scheduling compared with the existing control strategy. The graph also shows which controller is active at which times for GS.

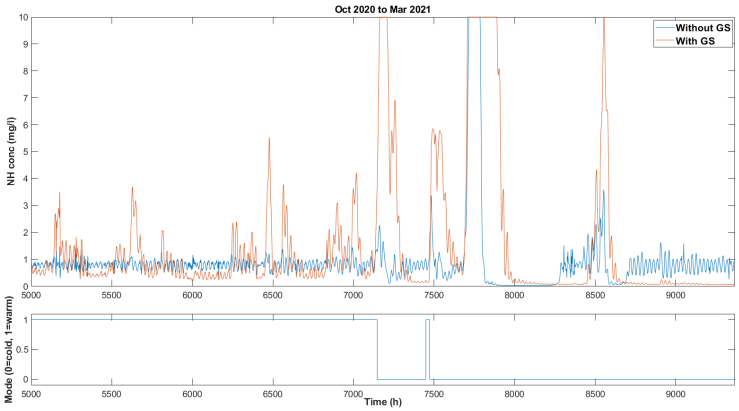

Figure 5.9: Comparison with and without GS during the period from October 2020 to March 2021. Bottom plot indicates which controller is active.

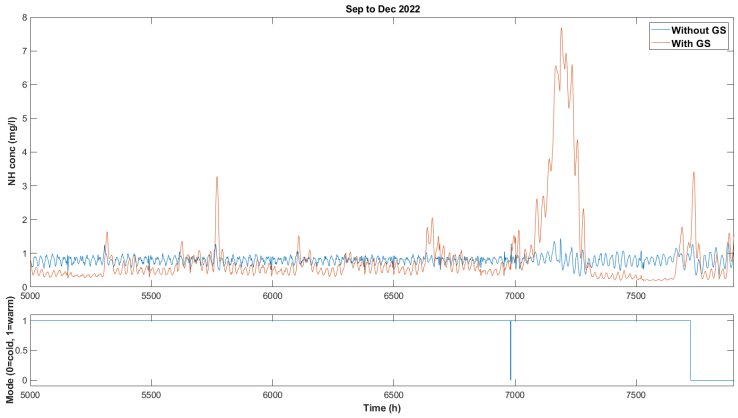

Figure 5.10: Comparison with and without GS during the period from September to December 2022. Bottom plot indicates which controller is active.

In the same way as for the feedforward control, the energy consumption was also calculated and is presented in Table 5.2

Table 5.2: Energy consumption for the above tested simulations.

	October 2020 to March 2021	September to December 2022
Without GS	518.15 MWh	341.08 MWh
With GS	421.53 MWh	336.23 MWh

5.4 Feedforward

Based on the step responses, the transfer functions from the inlet flow rate, inlet temperature, and control signal(DO) to the output signal (NH level) were found and can be seen in Equation (5.1), (5.2) and (5.3) respectively.

$$G_{yd,inflow} = \frac{0.031}{493s + 1} \tag{5.1}$$

$$G_{yd,temp} = \frac{2.76}{43s + 1} \tag{5.2}$$

$$G_{yu} = \frac{-21.4}{1.5s + 1} \tag{5.3}$$

The ideal feedforward compensators, calculated according to Equation (2.4) and are displayed in Equations (5.4) and (5.5) for feedforward of inlet flow rate and temperature, respectively.

$$G_{ff,inflow} = -\frac{0.031}{21.4}\frac{1.5s + 1}{493s + 1} \tag{5.4}$$

$$G_{ff,temp} = -\frac{2.76}{21.4}\frac{1.5s+1}{43s+1} \tag{5.5}$$

When tested on the design steps, they were however not found to work as intended. They were therefore tuned and the resulting feedforward compensators can be seen in Equations (5.6) and (5.7).

$$G_{ff,inflow} = -0.18 \cdot \frac{0.031}{21.4}\frac{10s+1}{35s+1} \tag{5.6}$$

$$G_{ff,temp} = 0.002 \cdot \frac{2.76}{21.4}\frac{10s+1}{10s+1} \tag{5.7}$$

Worth noting is that after the tuning of the compensators, they differ substantially from the ideal ones.

5.4.1 Time period from October 2020 to March 2021

The same time periods as for the model validation were utilized for the evaluation of the control systems. For the first time period from October 2020 to March 2021 the results are presented below. NH concentration in the outflow can be seen in Figure 5.11 for the feedforward compensator of inlet flow rate compared to the existing control structure without feedforward.

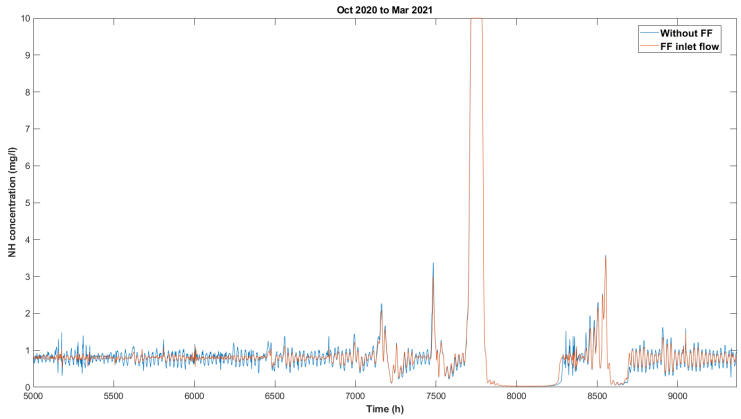

Figure 5.11: Comparison with and without feedforward of the inlet flow rate during the period from October 2020 to March 2021.

In Figure 5.12 the same comparison of the outgoing NH concentration is made but with the feedforward of temperature instead. The difference between the curves is negligible, resulting in them appearing as a single curve.

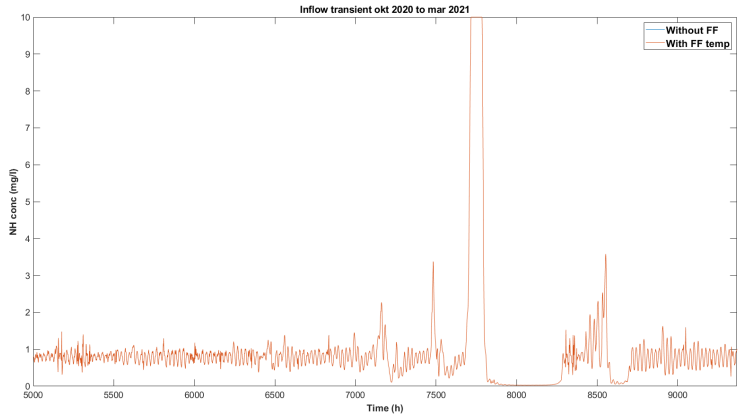

Figure 5.12: Comparison with and without feedforward of the temperature during the period from October 2020 to March 2021.

Figure 5.13 compares the DO setpoint between the simulations with and without feedforward of the inlet flow rate for a part of the time period.

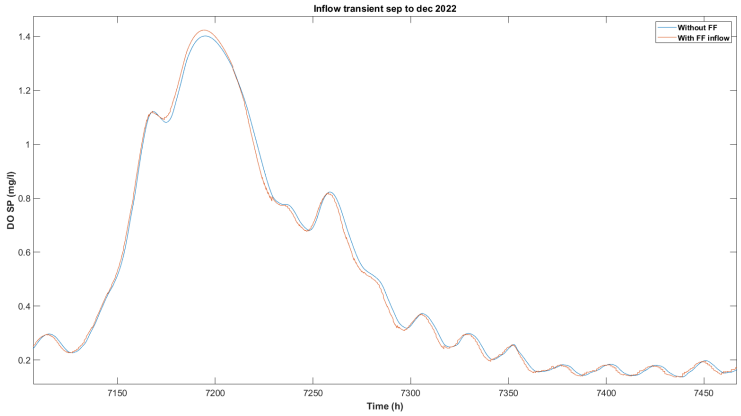

Figure 5.13: DO setpoint with and without feedforward of the inlet flow rate during the period from October 2020 to March 2021.

In Figure 5.14 the total airflow was compared between the existing control strategy and the feedforward of inlet flow rate for a limited time during the period.

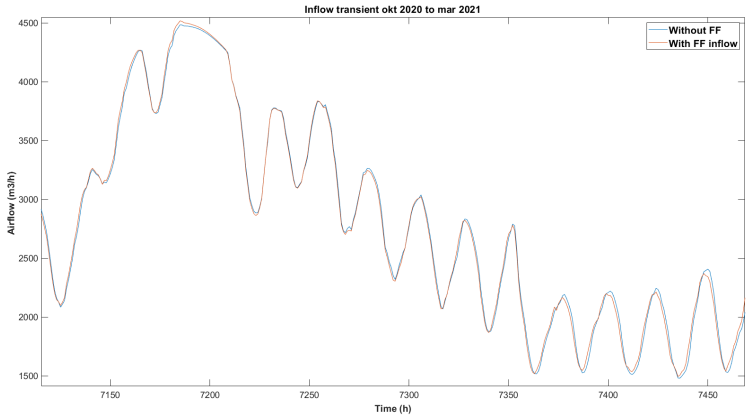

Figure 5.14: Total airflow with and without feedforward of the inlet flow rate during the period from October 2020 to March 2021.

5.4.2 Time period from September to December 2022

For the period from September to December 2022 the same comparisons as for the previous period was made. Similarly Figure 5.15 presents the comparison of outgoing NH concentration between the existing structure with the feedforward of inlet flow rate.

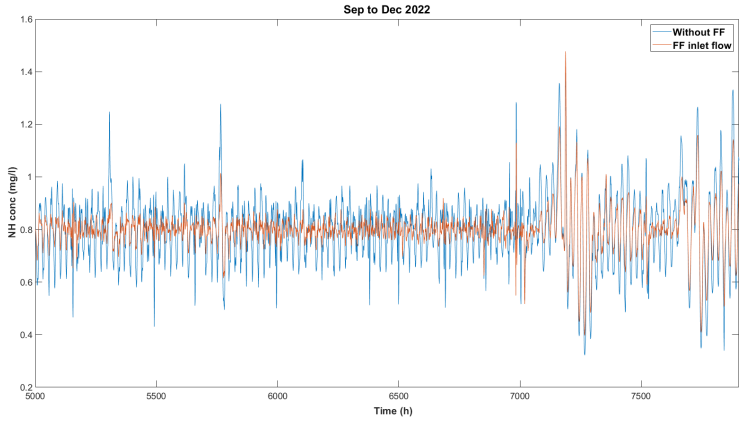

Figure 5.15: Comparison with and without feedforward of the inlet flow rate during the period from September to December 2022.

Figure 5.16 also shows the outgoing NH concentration for feedforward of temperature disturbance. In the same way as for the first time period, the difference between the temperature feedforward and existing system is negligible.

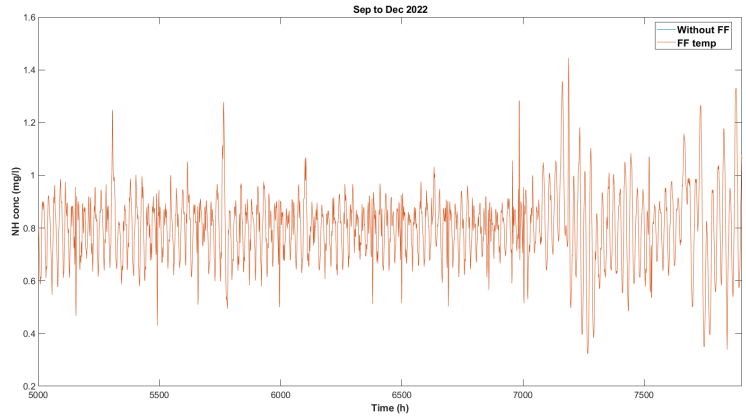

Figure 5.16: Comparison with and without feedforward of the temperature during the period from September to December 2022.

Figure 5.17 shows the DO setpoint for the feedforward of inlet flow rate.

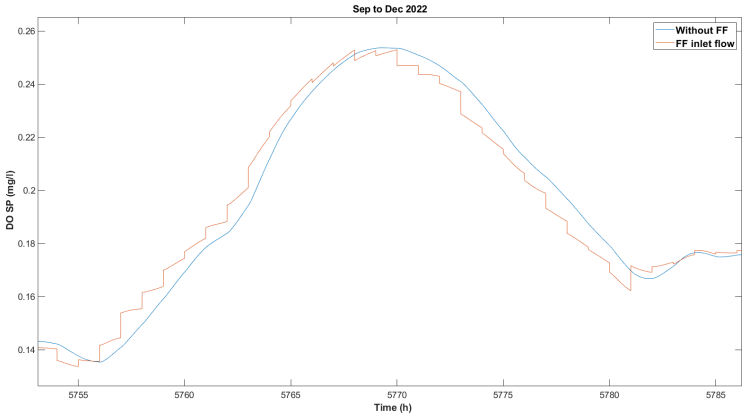

Figure 5.17: DO setpoint with and without feedforward of the inlet flow rate during the period from September to December 2022.

In Figure 5.18, the total airflow comparison between the feedforward of inlet flow rate and the existing system is seen.

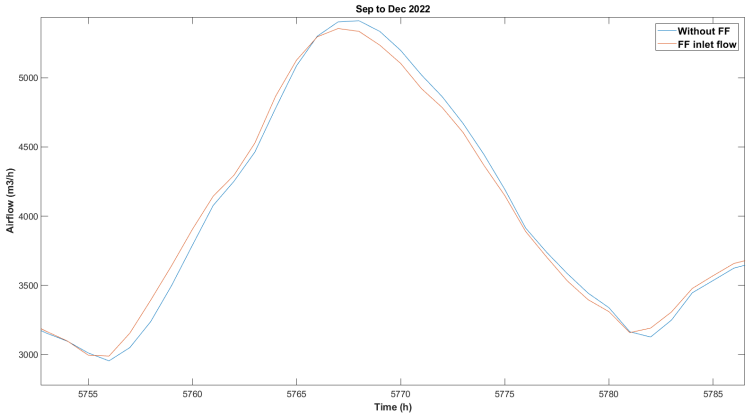

Figure 5.18: Total airflow with and without feedforward of the inlet flow rate during the period from September to December 2022.

For the above mentioned cases the energy consumption was also calculated. This is presented in Table 5.3.

Table 5.3: Energy consumption for the above tested simulations.

	October 2020 to March 2021	September to December 2022
Without FF	518.15 MWh	341.08 MWh
With FF inlet flow rate	514.48 MWh	341.02 MWh
With FF temp	518.15 MWh	341.08 MWh

6

Discussion

In this chapter the findings of this thesis are discussed. It is done with the thesis aim in mind.

6.1 Model validation

As can be seen in the comparisons in Section 5.1, the model captures the dynamics of the system for large transients, but there is a notable difference in amplitude in how well the model responds to the two transients examined. This could have multiple explanations, but besides the obvious reasons like model simplifications, etc. affecting the behavior, there is also the possibility that the inaccuracy of the ammonium sensor described in Section 3.2 means that the levels measured does not necessarily reflecting the actual level. Therefore, the possibility exists that some differences can be derived from the measurement inaccuracies.

One large simplification made in the model is that the temperature instantly affects all basins while in reality, there is a progression due to the hydraulic properties. This will in turn affect the dynamics, likely significantly. An improvement would therefore be to implement the effect of temperature so that this dynamic is taken into account. This could be done by implementing an energy balance for the wastewater treatment model, which would cause the water temperature to propagate through the system rather than updating instantaneously. This could prove to be extra important as the temperature has been shown to greatly impact the wastewater treatment process.

Beyond that, the main inconsistency that could be investigated is the significantly lower oxygen levels required for the model compared to the measured values of the real system. Or, from the other perspective the system outputs significantly lower ammonium levels when the DO levels are close to the measured ones. However, as previously stated the accuracy of the measurements must also be taken into consideration.

As mentioned earlier, one of the biggest problems with the design of model-based controllers is the settler model. Although it shows good accuracy, it does not ensure global stability of the whole system, which leads to problems designing model-based controllers and evaluating said controllers. Therefore, one of the most substantial improvements to the WWTP model would be a settler model that ensures global stability for the system while still maintaining good model accuracy.

6.2 LQG

Given that the state space of the system is neither observable nor controllable, an ASM1 system is almost always difficult to use for the development of a model-based controller system. Given that the model is not globally stable, due to the settler, as previously stated this creates a system that is neither detectable nor stabilizable, thus rendering the LQG solution ill-posed and unfit to control the plant. With modifications to the model, removing the settler and replacing it with a simple recirculation naturally results in a stable but incorrect system model. However, what this did was show the significant nonlinearities present in the biological system, such as the nitrification and denitrification equations shown in Equations (4.1a). (4.1i) as well as multiple other nonlinearities. This is demonstrated in Figure 5.8. LQG is a model-based control strategy which uses a linearized model as a basis for the control design is is essential that the system can be approximated as linear, at least in the operational range. This is clearly not the case, as observed in Figure 5.8. Therefore, the system proved to be too nonlinear to be able to be controlled by a linear model-based controller, even if a better settler model was discovered. This also gave insight that simpler controllers, such as PI (or PID) might perform better operate purely on the error between the reference and the output. Thus, they are able to function even for very nonlinear systems, as the controller does not depend on the system itself.

6.3 Gain scheduling

Based on the graphs from the two simulation cases, the gain scheduling solution handles the simulation tests worse than the current control setup. This results in spikes in effluent ammonia levels from the daily variations. The performance during the high ammonium spikes did not improve in the case for 2020-2021 and worse during the 2022 case. In the latter, however, the normal operations performance is better than in the former but still worse than the existing control system. Regarding energy consumption, the results are ambiguous with an increase for the 2020-2021 case and a decrease for the 2022 case. Unlike the FF case the GS shows a very large improvement in energy savings. However, this is likely just a result of the GS control system performing worse than the current system, thus reducing the energy consumption.

One possible explanation to the decreased performance of the gain scheduling solution is that the controller parameters used are not the best ones. Retuning could potentially increase performance, especially the controller for warm temperatures as it seems to perform worse than the cold one. However, retuning may not be very easy. During the process of controller design, it was hard to correctly identify the system parameters from the step responses which could explain why the resulting control parameters were not optimal. However, there is a problem with with obtaining good tuning data from the step tests. This can be observed in Figure 4.3, where the step starts of very steeply but then shifts into a slower ramping response. This is likely due to the fact that the system has both fast and slow dynamics, the

fast being the systems initial response to the higher/lower oxygen level while slower dynamics being a result the bacterial growth/decay. It is likely that these advanced dynamics cause problems for the PI controllers as they are tuned for a specific bacteria concentration but will experience a multitude of different concentrations when tested and perform better or worse accordingly. This is also likely the cause behind why lower levels of ammonia are measured for multiple days following a large ammonia spike, this can be seen in Figures 5.9 and 5.10. The reasoning being that the bacteria levels have had time to adapt to the high ammonia levels during the spike and are therefore over-consuming ammonia once the spike has ended. To conclude it is possible that the GS control design could be tuned to perform better than it currently does, but this would likely need to be done with another method than the Lambda method, but no matter the tuning method a PI controller will likely struggle to handle the different bacteria concentrations that occur during operations.

6.4 Feedforward control

The results of implementing feedforward control show that for the inlet flow rate it is possible to achieve improvement in both the disturbance rejection and the energy consumption, but the effect is small in terms of energy consumption. For disturbance rejection of daily variations during normal load conditions, the improvement was more noticeable and will be discussed further below. However, it did not lower the high ammonia spikes during the periods tested. For the temperature feedforward, the difference was minimal in all aspects compared to the current control strategy. This means that the savings of implementing the feedforward control system are low if any. Without a proper economic analysis it is hard to say if it would result in economic savings.

It is hard to say exactly what is causing the spikes in ammonia level but as there seems to be no improvement with change of control systems that it is most likely not the reason. One theory is that there is a maximum limit on how much ammonia the system can mitigate, due to the characteristics of the system such as residence time, bacterial growth, consumption speed of ammonia etc. Therefore, the ability to control the system based solely on the oxygen level in the water is only feasible up to a certain operating point, which likely varies with external factors such as temperature and inlet flow rate. That would mean that in order for the control system to be able to counter any large transients, the treatment plant would need to be dimensioned for a much higher capacity. That does however come at a cost for construction but it would also mean that a larger volume of water needs to be aerated if no control of the aerated volume. This can be done by running different number of aeration basins depending on situation is implemented. It is possible that this could lead to a higher energy consumption but it is hard to say without proper investigation. However, it is not certain that the benefits of increased capacity are larger than the drawbacks as the high levels of ammonia that is seen in the test cases are relatively rare. The plant also has, to a limited extent, the possibility of controlling the inlet flow rate by, for example, using sewer tunnels as storage and thereby smoothening the increase in inlet flow rate.

The control input is in this case the DO setpoint and in Figures 5.13 and 5.17 can be seen that with feedforward of inlet flow rate, the response in control signal comes earlier than for the existing system. The peaks are also slightly lowered. This is exactly how a feedforward control is supposed to work so it is positive to see. As mentioned previously, it has an noticeable effect on the outgoing NH concentration but the effect on energy consumption is not clear. During the first period there is a small decrease but during the second no significant decrease can be seen and therefore the conclusion that feedforward of inlet flow rate lowers energy consumption cannot be drawn.

It is also important to address the effect of feedforward on the total airflow in the system which is closely related to the DO setpoint. A visual comparison with the existing system shows that, for the feedforward of inlet flow rate in both simulated time periods, the impact is marginal. If anything, the airflow graph is somewhat smoothened for both time periods. That is good because a more stable outlet concentration of ammonium may come at the cost of larger changes in airflow, i.e. a more aggressive control input. As that might trigger the need for starting and stopping some blowers to provide the right amount of air that would be against the scope of the project, as mentioned in Section 4.1.3. While the performance is better, the improvement is not large as indicated by the energy consumption mentioned earlier.

While the performance is not worse, as previously noted, the improvement is marginal. Therefore, it can not be argued from the results in this report that a more favorable operating pattern of the blowers has been obtained. To conclude that, a more detailed analysis of the blowers is needed, which takes the individual capacities of the blowers into account and in which order they are used.

6.5 Future work

The gain scheduling method could be implemented in other ways, such as a schedule between different LQR controllers. The difficulty would not be in designing the controllers, as that can be done quite simply, rather it would be finding different points of operations and scheduling between the controllers in a way that does not lead to instabilities or other unwanted behaviors.

With these results as a foundation, numerous future works can be done. One clear approach to deal with the nonlinearities of the system would be to try employing a nonlinear controller, this would however likely be very computationally intensive as well as a complex task due to the ASM1 models large number of states and uncertainty. Another possibility would be to use a model predictive controller, which could help better adapt to the complex system. This is supported by the system being slow, making the controller less computationally intensive. However, this would likely require a globally stable model. An alternative, and possibly more feasible approach would be to identify a data-driven model, ignoring the high-dimensional, complex internal state dynamics that arise when modeling the wastewater treatment system. By utilizing the large amounts of historical data that exists, combined with either machine learning or system identification techniques, it could be possible to

construct a model that captures the dynamics of the system without knowledge of the inner workings. Such a model would be difficult to generalize to other applications compared a physical modeling approach as it is easier to interpret the physical meaning and underlying mechanisms of such a model. One key advantage of a data-driven model would be that it likely would be more robust and less sensitive to model uncertainties as it is not built on model assumptions in the same way as the physical model.

It should be noted that all of the results were tested on the model of the real system, which while determined to be sufficiently good still included some major deviations from the real system, such as the lower oxygen levels in the model compared to the measured values in the real system. Such deviations can negatively affect the comparative results, making them less reliable.

7

Conclusion

A WWTP is a complex dynamical system, often modeled with the ASM1 model, so was the case for this project. Given the nonlinearities and that the system is neither controllable nor observable, it was not possible to design a working model-based LQG controller. Simpler controllers proved to be a better choice. In order for a model-based controller to work, it would likely need to be more complex than an LQG controller, for example, a nonlinear controller of some sort.

The GS solution showed improvements in energy consumption but with a substantial decrease in performance, even though the daily levels of NH were lower than those of the existing system. Most probably, the problem lies in the tuning of the controllers. Due to the split dynamics of the system, with a fast response of oxygen level but a slower response of bacterial growth, it was hard to tune the controllers properly.

Feedforward proved, in the case of the inlet flow rate, to yield a better performance in terms of daily variations. This improvement could not be seen with the feedforward of temperature. In neither of the two cases, the large spikes in effluent ammonia level could be mitigated. Therefore, these are likely caused by capacity constraints in the system. An example of such constraint could be the residence time becoming too short due to the large increase of the inlet flow rate. In order to solve these problems, an increase of the capacity of the plant is likely needed.

Bibliography

[1] A. Lingsten and M. Lundkvist, "Swedish water and wastewater utilities use of energy in 2008," 2011.

[2] S. Bengtsson, D. Fujii, M. Arnell, S. Andersson, B. Carlsson, H. Held, and D. Gustavsson, "Effektiv luftning Design, drift, underhåll och upphandling av luftningsutrustning för kommunala avloppsreningsverk," tech. rep., Svenskt Vatten Utveckling, 2019.

[3] L. Åmand, *Ammonium Feedback Control in Wastewater Treatment Plants*. PhD thesis, Uppsala University, 4 2014.

[4] T. E. Jenkins, *Aeration Control System Design : A Practical Guide to Energy and Process Optimization.* John Wiley & Sons, Incorporated, 2013.

[5] C.-F. Lindberg, *Control and estimation strategies applied to the activated sludge process*. Uppsala University Stockholm, Sweden, 1997.

[6] R. O. Mines, *Environmental Engineering : Principles and Practice.* John Wiley & Sons, Incorporated, 2014.

[7] F. Garcia-Ochoa and E. Gomez, "Bioreactor scale-up and oxygen transfer rate in microbial processes: An overview," *Biotechnology Advances*, vol. 27, pp. 153–176, 3 2009.

[8] M. Hovd, "Advanced Chemical Process Control - Putting Theory into Practice," p. 326, 2023.

[9] K. Forsman, *Reglerteknik för processindustrin*. Lund: Studentlitteratur, 1:4 ed., 2005.

[10] K. J. Åström and T. Hägglund, *Advanced PID control*. ISA-The Instrumentation, Systems, and Automation Society, 2006.

[11] F. Bruzelius, *Linear Parameter-Varying Systems an approach to gain scheduling*. PhD thesis, Chalmers University of Technology, 2004.

[12] T. Glad, *Control theory: multivariable and nonlinear methods / Torkel Glad and Lennart Ljung.* Taylor & Francis, 2000.

[13] G. Strang, *Introduction to Linear Algebra*. Wellesley, MA: Wellesley-Cambridge Press, 5th ed., 2016.

[14] G. Meinsma and A. van der Schaft, *A Course on Optimal Control*. Springer Undergraduate Texts in Mathematics and Technology, Cham: Springer Nature Switzerland, 2023.

[15] Käppalaförbundet, "Reningsprocessen," 2025.

[16] M. Henze, C. P. L. Grady Jr, W. Gujer, G. v. R. Marais, and T. Matsuo, "Activated sludge model No.1," *Wat Sci Technol*, vol. 29, 1 1987.

[17] I. Takács, G. G. Patry, and D. Nolasco, "A dynamic model of the clarification-thickening process," *Water Research*, vol. 25, pp. 1263–1271, 10 1991.

[18] J. Monod, "THE GROWTH OF BACTERIAL CULTURES," *Annual Review of Microbiology*, vol. 3, pp. 371–394, 10 1949.

[19] K. V. Gernaey, M. C. Van Loosdrecht, M. Henze, M. Lind, and S. B. Jørgensen, "Activated sludge wastewater treatment plant modelling and simulation: state of the art," *Environmental Modelling & Software*, vol. 19, pp. 763–783, 9 2004.

[20] P. Dold and M. Fairlamb, "Estimating oxygen transfer KLa, SOTE and air flow requirements in fine bubble diffused air systems," *Proceedings of the Water Environment Federation*, vol. 2001, pp. 780–791, 1 2001.

[21] P. Paul, "Assessing the influence of pronounced diurnal temperature variations in nontemperate zones on the denitrification/nitrification rate using the C OST Benchmark activated sludge model no. 1 simulation.," *Water & Environment Journal*, vol. 28, pp. 526–532, 12 2014.

[22] T. Wik and B. Lindén, "Modeling, control and simulation of recirculating aquaculture systems," *IFAC Proceedings Volumes*, vol. 37, no. 3, pp. 141–146, 2004. 9th IFAC International Symposium on Computer Applications in Biotechnology 2004 (CAB 9), Nancy, France, 28-31 March 2004.

[23] K. J. Åström and T. Hägglund, *4.5.1 λ-Tuning*. International Society of Automation (ISA), 1995.

A

Model Parameters

Summary of the model parameters used for the WWTP model. The ASM1 model parameters as well as the settler parameters are displayed in Table A.4. The modeling parameters used for the oxygen transfer model are presented in Table A.1 and the parameters for the temperature dependencies in Table A.2. The correction factors α and β are presented in Table A.3.

	Basin			
Parameter	1	2	3	4
$DD(\%)$	6.7	5.3	3.9	3.0
$k_1(\frac{1}{d})$	4.7	2.0	1.0	0.9
$k_2(\frac{1}{d})$	0.6	0.6	0.6	0.4
Y	0.75	0.85	1.0	1.0

Table A.1: Parameter values for the oxygen transfer model

Parameter	Value
θ_{μ_H}	0.0069
θ_{μ_A}	0.0098
θ_{k_H}	0.11
θ_{k_A}	0.069
θ_{b_H}	0.069
θ_{b_A}	0.08
θ_{K_La}	1.024

Table A.2: Temperature correction factors[21][2].

Parameter	Value
α	0.5
β	0.95

Table A.3: Correction factors for K_La and DO_{sat} respectivly

Table A.4: ASM1 and settler model parameters[3].

Description	Notation	Unit	Value
Autotrophic yield	Y_A	gcell/gN	0.24
Heterotrophic yield (aerobic conditions)	Y_H	gcell/gCOD	0.67
Heterotrophic yield (anoxic conditions)	Y_H	gcell/gCOD	0.54
Fraction of biomass yielding to particulate products	f_p	-	0.08
Nitrogen content in biomass	i_{XB}	gN/gCOD	0.086
Nitrogen content in products from biomass	i_{XP}	gN/gCOD	0.06
Maximum heterotrophic growth rate	$\mu_{max,H}$	d^{-1}	6
Half-saturation coefficient for heterotrophic biomass	K_S	$gCOD/m^3$	20
Oxygen half-saturation constant for heterotrophic biomass	K_{OH}	gO_2/m^3	0.2
Nitrogen half-saturation constant for heterotrophic biomass	K_{NO}	$gNO_3 - N/m^3$	0.5
Decay coefficient for heterotrophic biomass	b_H	d^{-1}	0.22
Correction factor for anoxic growth of heterotroph	η_g	-	0.8
Correction factor for anoxic hydrolysis	η_h	-	0.4
Maximum specific hydrolysis rate	k_h	gCOD/gcell,d	3
Half-saturation constant for hydrolysis of slowly biodegradable substrate	K_X	gCOD/gcell	0.03
Maximum autotrophic growth rate	$\mu_{max,A}$	d^{-1}	0.8
Ammonium half-saturation coefficient for autotrophs	K_{NH}	$gNH_3 - N/m^3$	1.0
Oxygen half-saturation coefficient for autotrophs	K_{OA}	gO_2/m^3	0.4
Ammonification rate	k_A	$m^3/gCOD, d$	0.08
Autotrophic decay rate	b_A	d^{-1}	0.05
Practical max. sed. velocity	v_0	m/h	250
Theoretical max. sed. velocity	v_0'	m/h	474
Sedimentation parameter, hindered zone	r_h	m^3/g	$8.5{\cdot}10^{-4}$
Sedimentation parameter, flocculent zone	r_p	m^3/g	$4.5{\cdot}10^{-3}$
Non settleable fraction	f_{ns}	g/m^3	$2.28{\cdot}10^{-3}$

DEPARTMENT OF ELECTRICAL ENGINEERING
CHALMERS UNIVERSITY OF TECHNOLOGY
Gothenburg, Sweden
www.chalmers.se

CHALMERS
UNIVERSITY OF TECHNOLOGY